A hypothalamic novelty signal modulates hippocampal memory

Shuo Chen, Linmeng He, Arthur J y Huang, Roman Boehringer, Vincent Robert, Marie Wintzer, Denis Polygalov, Adam Z Weitemier, Yanqiu Tao, Mingxiao Gu, et al.

HAL Id: inserm-02978755
https://inserm.hal.science/inserm-02978755

Submitted on 26 Oct 2020

A hypothalamic novelty signal modulates hippocampal memory

Shuo Chen[1]*, Linmeng He[1,2], Arthur J.Y. Huang[1], Roman Boehringer[1], Vincent Robert[3], Marie E. Wintzer[1], Denis Polygalov[1], Adam Z. Weitemier[1], Yanqiu Tao[1], Mingxiao Gu[1], Steven J. Middleton[1], Kana Namiki[4], Hiroshi Hama[4], Ludivine Therreau[3], Vivien Chevaleyre[3,5], Hiroyuki Hioki[6], Atsushi Miyawaki[4,7], Rebecca A. Piskorowski[3,5], Thomas J. McHugh[1,2]*

[1]Laboratory for Circuit and Behavioral Physiology, RIKEN Center for Brain Science, Wakoshi, Saitama, Japan.

[2]Department of Life Sciences, Graduate School of Arts and Sciences, The University of Tokyo, Tokyo, Japan.

[3]Université de Paris, Institute of Psychiatry and Neuroscience of Paris INSERM UMRS1266, 102-015 rue de la santé, 75014 Paris France.

[4]Laboratory for Cell Function and Dynamics, RIKEN Center for Brain Science, Wakoshi, Saitama, Japan.

[5]GHU PARIS Psychiatry and Neuroscience, 75014 Paris, France.

[6]Department of Cell Biology and Neuroscience, Juntendo University Graduate School of Medicine, Tokyo, Japan.

[7]Biotechnological Optics Research Team, RIKEN Center for Advanced Photonics, Wakoshi, Saitama, Japan.

*Corresponding author. E-mail: shuoshu@gmail.com (S.C.), thomas.mchugh@riken.jp (T.J.M.)

The ability to recognize information incongruous with previous experience is critical for survival, thus novelty signals in the mammalian brain have evolved to enhance attention, perception and memory[1-3]. Although the importance of regions such as the ventral tegmental area[4-6] and locus coeruleus[6,7] in broadly signaling novelty has been well established, these diffuse monoaminergic transmitters have yet to be shown to convey specific information regarding the type of stimuli that drive them[6]. Whether distinct types of novelty, such as contextual and social novelty, are differently processed and routed in the brain remain unclear. Here we identify a novelty hub in the hypothalamus – the supramammillary nucleus (SuM)[8]. Unique about this region is that it not only responds broadly to novel stimuli, but segregates and selectively routes different types of information to discrete cortical targets, the dentate gyrus (DG) and CA2 fields of the hippocampus, for the modulation of mnemonic processing. Taking advantage of a novel SuM-Cre transgenic mouse, we found that DG-projecting SuM neurons are activated by contextual novelty while the SuM-CA2 circuit is preferentially activated by novel social encounters. Circuit-based manipulation demonstrated that divergent novelty channeling in these projections significantly modifies hippocampal-based contextual or social memory. This content-

32　**specific routing of novelty signals represents a previously unknown mechanism that**

33　**enables the hypothalamus to flexibly modulate select components of cognition.**

34　The hypothalamus supports evolutionary conserved functions, including the regulation of

35　homeostatic states and innate behaviors[9]. However, given both the conservation of a behavioral

36　novelty response across species and the hypothalamic connections with the hippocampus, this

37　region may play a role in detecting novelty and influencing higher cognitive processing. Thus,

38　we conducted a systematic examination of the expression of c-Fos, a marker of active neurons, in

39　the hypothalamus of mice exposed to two omnipresent types of novelty, contextual and social

40　(Fig. 1a). While c-Fos expression increased in multiple hypothalamic regions, the SuM, a small

41　nucleus with direct projections to hippocampus[8], exhibited a remarkably high response to both

42　contextual[10,11] and social novelty (Fig. 1b and Extended Data Fig. 1), with similar proportions of

43　neurons activated in both conditions (Fig. 1c, novel context: 117.9 ± 4.1 c-Fos+ cells/mm^2; novel

44　animal: 129.9 ± 5.4; familiar context (control): 24.0 ± 2.5). To physiologically characterize the

45　novelty response of SuM neurons, we performed *in vivo* single-unit recordings in behaving mice

46　(Fig. 1d, e and Extended Data Fig. 2a–c). Each session consisted of exposure to a familiar

47　context, a novel context and finally a novel animal (Fig. 1d). A total of 141 well-isolated units

48　were recorded, comprised of 119 putative excitatory neurons (pEN, 84.4%) and 22 putative fast-

49　spiking interneurons (pIN, 15.6%). The average firing rate of all pEN units was significantly

50　higher during exposure to a novel context (2.5 Hz) or a novel social encounter (2.6 Hz)

51　compared to familiar contexts (2.1 Hz; Fig. 1f, g), whereas pIN units showed no significant

52　novelty modulation (Extended Data Fig. 2d–h). Subsets of pEN units significantly increased their

53　activity in response to contextual novelty (21.8%, 26 of 119 units) and social novelty (21.0%, 25

54　of 119 units), outweighing the subsets that showed decreased firing rates (8.4%, 10 of 119 units

55　for contextual; 0.8%, 1 of 119 units for social; Fig. 1h, i). Notably, a large portion of SuM

56　neurons (69.2%, 27 of 39 units) were specifically excited by one type of novelty but inhibited or

57　non-responsive to the other (Fig. 1f, j). Both the context and social driven populations displayed

58　a monotonic decrease in firing rates over time (Fig. 1k), suggesting uniform habituation of the

59　novelty response.

60　The SuM and related circuits have been difficult to study due to their small size and diverse cell

61　types[8]. Therefore, we developed a novel transgenic mouse line, Csf2rb2-Cre, to gain precise

62 genetic access to the SuM (SuM-Cre mouse; Fig. 2 and Extended Data Fig. 3). The pattern of

63 Cre expression in this line, confirmed by crossing with a *β*-gal Cre reporter line[12] (Extended Data

64 Fig. 3c, d), recapitulated the endogenous Csf2rb2 pattern[13], with robust expression in neurons of

65 the SuM. Injection of Cre-dependent adeno-associated virus (AAV) vector expressing eYFP into

66 the SuM resulted in a SuM-restricted signal (Fig. 2a, b) and strong terminal labeling in the

67 pyramidal layer of CA2 and the granule cell layer of the DG in the hippocampus[8] (Fig. 2a, c and

68 Extended Data Fig. 4). We further used tissue clearing techniques (Sca*l*eS)[14] to image SuM

69 projections in the whole brain and observed axons extending through the fornix superior and the

70 fimbria to a wide dorsal-ventral range of DG and CA2 (Extended Data Fig. 5).

71 To ask if these pathways are anatomically segregated, we simultaneously injected Cre-dependent

72 retrograde AAVs expressing eYFP and mCherry into the DG and CA2 of single mice (Fig. 2d, e

73 and Extended Data Fig. 6a). The majority of the identified SuM neurons were found to project

74 solely either to the DG ($37.3 \pm 2.2\%$, $N = 6$ mice, $n = 2{,}700$ neurons) or CA2 ($39.4 \pm 3.8\%$, $N = 6$

75 mice, $n = 2{,}700$ neurons) with less than a quarter ($23.3 \pm 2.7\%$, $N = 6$ mice, $n = 2{,}700$ neurons)

76 dually infected (Fig. 2e). The high viral titer and proximity of the CA2 and DG injection sites

77 raised the possibility that the dually infected population could be overestimated; thus we injected

78 small volumes of Alexa Fluor 488 and Alexa Fluor 594 cholera toxin subunit B (CTB) into the

79 DG and CA2, respectively, and found a very small fraction of doubly labeled neurons[15] ($2.6 \pm$

80 0.5%, $N = 3$ mice, $n = 708$ neurons, Extended Data Fig. 6b). Further, single injections of

81 retrograde AAV into CA2 or DG revealed robust fibers only in the injection region, with no

82 collaterals or synaptic transmission detected in the other (Extended Data Fig. 7a–d), confirming

83 that these pathways are largely segregated.

84 We next asked if novelty-driven SuM neurons project to hippocampus and whether novelty

85 information with distinct features, e.g. contextual and social, is differentially routed. We bred the

86 SuM-Cre mice with the Tet-Tag mouse line[16], carrying the c-Fos-tTA transgene to permit long-

87 term tagging of c-Fos activity in the SuM (Fig. 3a–d). These mice allowed dual-color labeling of

88 temporally segregated active SuM ensembles, visualized by c-Fos-triggered viral eYFP

89 expression (green) and anti-c-Fos immunohistochemistry (red), respectively. Consistent with our

90 electrophysiological results, sequential presentation of two different types of novelty revealed

91 significant segregation of active ensembles (Fig. 3c, d). For simultaneous circuit tracing and c-

3

92   Fos labeling, we injected retrograde AAVs expressing mCherry either into the DG or CA2 and

93   AAV-TRE-DIO-eYFP into the SuM of the double-transgenic mice (Fig. 3e–j). Significantly

94   higher c-Fos activity was observed in the DG-projecting population compared to the CA2-

95   projecting population in mice exposed to contextual novelty (Fig. 3j, DG-projecting: $39.2 \pm 1.8\%$

96   versus CA2-projecting: $16.3 \pm 1.1\%$). In contrast, in mice exposed to a novel social stimulus, c-

97   Fos expression was significantly elevated in the CA2-projecting neurons compared to the DG-

98   projecting ones (Fig. 3j, CA2-projecting: $32.8 \pm 2.2\%$ versus DG-projecting: $12.4 \pm 1.1\%$).

99   Similar results were observed when anti-c-Fos immunohistochemistry was used to assay activity

100   in SuM-Cre mice injected with retrograde AAVs either into the DG or CA2 for circuit labeling

101   (Extended Data Fig. 8a–f).

102   To validate this novelty-specific projection bias, we conducted *in vivo* single unit recordings in

103   the SuM (Fig. 3k–t). Single-unit activity was recorded in the SuM during low-frequency laser

104   stimulation to induce antidromic spikes in mice with ChR2 expression in the SuM and optic

105   fibers above DG and CA2 (Fig. 3l–q and Extended Data Fig. 8g–l), permitting projection-

106   specific optogenetic identification of SuM neurons. The majority of the DG-projecting neurons

107   (10 of 12 units) increased their firing rate in a novel context (Fig. 3r, example cells 1 and 2) and

108   the average firing rate change across the population was higher with novel contextual exposure

109   than during novel social exposure (Fig. 3s, contextual: 0.39 versus social: 0.13). In contrast, most

110   CA2-projecting neurons (15 of 17 units) exhibited a larger firing rate increase in response to

111   social novelty than to contextual novelty (Fig. 3r, example cells 3 and 4; Fig. 3t, social: 0.43

112   versus contextual: 0.18).

113   The novelty-selective activation of the SuM-DG and SuM-CA2 circuits led us to assess whether

114   manipulation of either circuit impacts hippocampal memory in a feature (contextual or social)-

115   dependent way. We employed optogenetics to dissect the two circuits by delivering light to axon

116   terminals in either the DG or CA2 (Fig. 4; Extended Data Fig. 7). Contextual behavior was

117   assessed using a one-day habituation protocol in a novel high-walled enclosure (Fig. 4a and

118   Extended Data Fig. 9). Following three habituation sessions (A1–A3), across which all groups

119   decreased exploration (Fig. 4b–e) indicating familiarization to the environment[17], light was

120   delivered to SuM terminals in the hippocampus (Session A4 in Fig. 4a). Only mice in which the

121   SuM-DG pathway was activated altered their behavior, increasing exploration compared to the

122   controls (Fig. 4b, relative travel distance: 58.1 ± 3.4% versus 39.6 ± 5.6%), consistent with an

123   increased perception of contextual novelty. We then altered the now familiar context by

124   displacing the local objects and changing the visual cues on the walls (Session B1 in Fig. 4a,

125   Extended Data Fig. 9a). Control mice reacted to this contextual novelty by increasing their

126   exploration during the session, however this response was absent in mice in which the SuM

127   terminals in the DG were inhibited (Fig. 4c, relative traveling distance: DG/eNpHR: 38.1 ± 4.6%

128   versus DG/EYFP: 71.6 ± 3.8%), suggesting a deficiency in contextual novelty recognition. A

129   final session (B2) in the altered context in the absence of light confirmed that once relieved from

130   SuM-DG inhibition the mice could recognize the contextual change (Fig. 4c). Identical sets of

131   experiments were performed with ChR2- or eNpHR-transfected mice in the absence of light

132   delivery and no changes were found in behavior (Extended Data Fig. 9f–i). These results

133   demonstrate that the novelty signal routed by the SuM to DG projection can modulate behavior

134   based on hippocampal contextual memory.

135   Next we employed a direct interaction test to explore the impact of SuM inputs on social

136   memory (Fig. 4f–k). Subject mice were first exposed to a novel mouse without light stimulation

137   and interaction time was scored. One hour later mice were either re-exposed to the same mouse

138   or exposed to a second novel mouse, with light delivered to the DG or CA2. In CA2-targeted

139   mice we found that photostimulation caused a deficit in the expression of social memory, as

140   these mice exhibited high levels of social interaction, resulting in a significantly higher

141   habituation index compared to the controls (Fig. 4h, CA2/ChR2: 0.116 ± 0.081 versus

142   CA2/eYFP: −0.373 ± 0.103). Optogenetic manipulations targeting the DG, regardless of

143   stimulation or inhibition, showed no effect on social interaction (Fig. 4g, j). These data suggest

144   that the SuM to CA2 pathway can drive social novelty-linked exploratory behavior and routes

145   social instead of contextual novelty to the hippocampus.

146   To understand how these projections influence the hippocampus we examined how the two

147   discrete SuM-hippocampal circuits differ in neurotransmission (Extended Data Figs. 6c–h and

148   10). Multiplex fluorescence *in situ* hybridization (RNAscope, Extended Data Fig. 6c–h) in mice

149   injected with retrograde AAVs expressing eYFP into the DG or CA2 found that while Cre

150   recombination occurs in both glutamatergic and GABAergic neurons, the majority of DG-

151   projecting neurons are positive for both VGLUT2 and VGAT[15,18,19], whereas most CA2-

projecting neurons are only VGLUT2+. Consistent with this, whole cell voltage-clamp recordings in acute hippocampal slices (Extended Data Fig. 10) revealed DG-projecting SuM neurons simultaneously release both glutamate and GABA (Extended Data Fig. 10f–j)[15,18,19], while SuM-CA2 transmission is entirely glutamatergic (Extended Data Fig. 10k–o). While both inputs induced modest excitatory post-synaptic currents (EPSCs) in their target hippocampal principal neurons, they shared a robust feed-forward inhibitory component, evidenced by the large inhibitory post-synaptic currents (IPSCs) seen in DG granule cells (GCs) or CA2 pyramidal neurons (PNs) upon SuM axon stimulation. This regulation of the local excitation/inhibition (E/I) balance in the hippocampus has been speculated to contribute to the fine tuning of neuronal excitability and the dynamic range of neuroplasticity during mnemonic processing[19-21]. Thus, SuM transmission may provide an alternative and highly flexible mode of novelty signaling for shaping hippocampal encoding, in complement to the modulatory effects of monoaminergic innervation.

To better understand how the wide anatomical connectivity[8] of the SuM underlies this signaling we used projection-specific tracing to profile upstream inputs to the DG- and CA2-innervating SuM neurons (Extended Data Fig. 11). Both populations receive extensive inputs from subcortical regions, and although there were no significant statistical differences, inputs to the DG-projecting population were skewed towards brain regions in the reward and motor systems, while the CA2 projectors received proportionally more inputs from neurons in socially engaged regions, particularly the paraventricular hypothalamic nucleus[22] and medial preoptic area[23] (Extended Data Fig. 11g, h). This projection-specific connectivity may underlie the ability of the SuM to segregate contextual and novelty signals. In contrast to these diverse inputs, the ascending outputs of the hippocampal projecting SuM neurons are fairly restricted to the hippocampus (Extended Data Figs. 4 and 5). Therefore, the SuM may integrate internal states with cognitive input, extracting the contextual and social salience of stimuli and routing this signal for the modulation of mnemonic processing.

The observed selectivity of the SuM-DG and SuM-CA2 circuits supports the idea of specialized information processing along the longitudinal axis of the hippocampus[24]. The DG[25-27] can rapidly detect and encode contextual changes, while the loss of synaptic plasticity in DG GCs impairs context discrimination and novelty recognition[28,29] but not social memory[30]. Therefore,

182 the SuM input to DG GCs, via regulation of local E/I balance, may serve as a key facilitator of

183 plasticity at the perforant pathway when new contextual information is encoded[19]. In contrast,

184 interventions targeting pyramidal cells in CA2 have no impact on contextual learning, but rather

185 result in profound changes in social memory[31-36]. We found that activation of the SuM input in

186 CA2, which engages strong feed-forward inhibition (Extended Data Figs. 10), could induce a

187 social novelty response (Fig. 4h), however inhibition could not impair an endogenous response

188 (Fig. 4k), suggesting redundancy in this circuitry. We speculate that the SuM inputs to dorsal

189 CA2 may shift local E/I balance and modulate downstream information flow in the hippocampus

190 that favors the encoding of new social information in its ventral subregions.

191 Our work provides mechanistic evidence for a hypothalamic content-specific novelty signal that

192 can contribute to shaping the engagement of distinct hippocampal subregions during encoding of

193 different types of memory. SuM modulation is probably not the sole source of such distinct

194 specificity; however, our findings demonstrate that within this small hypothalamic nucleus,

195 distinct novelty features can be detected, segregated and transmitted. How differences in input

196 circuitry permit novelty segregation in the SuM and how the signaling of segregated novelty

197 modifies hippocampal activity on the physiological level during behavior await further

198 investigation.

199

200   1   Ranganath, C. & Rainer, G. Neural mechanisms for detecting and remembering novel events. *Nat*
201   *Rev Neurosci* **4**, 193-202, doi:10.1038/nrn1052 (2003).
202   2   van Kesteren, M. T., Ruiter, D. J., Fernandez, G. & Henson, R. N. How schema and novelty
203   augment memory formation. *Trends Neurosci* **35**, 211-219, doi:10.1016/j.tins.2012.02.001
204   (2012).
205   3   Kafkas, A. & Montaldi, D. How do memory systems detect and respond to novelty? *Neurosci*
206   *Lett* **680**, 60-68, doi:10.1016/j.neulet.2018.01.053 (2018).
207   4   Lisman, J. E. & Grace, A. A. The hippocampal-VTA loop: controlling the entry of information
208   into long-term memory. *Neuron* **46**, 703-713, doi:10.1016/j.neuron.2005.05.002 (2005).
209   5   McNamara, C. G., Tejero-Cantero, A., Trouche, S., Campo-Urriza, N. & Dupret, D.
210   Dopaminergic neurons promote hippocampal reactivation and spatial memory persistence. *Nat*
211   *Neurosci* **17**, 1658-1660, doi:10.1038/nn.3843 (2014).
212   6   Duszkiewicz, A. J., McNamara, C. G., Takeuchi, T. & Genzel, L. Novelty and Dopaminergic
213   Modulation of Memory Persistence: A Tale of Two Systems. *Trends Neurosci*,
214   doi:10.1016/j.tins.2018.10.002 (2018).
215   7   Takeuchi, T. *et al.* Locus coeruleus and dopaminergic consolidation of everyday memory. *Nature*
216   **537**, 357-362, doi:10.1038/nature19325 (2016).
217   8   Pan, W. X. & McNaughton, N. The supramammillary area: its organization, functions and
218   relationship   to   the   hippocampus.   *Prog   Neurobiol*   **74**,   127-166,
219   doi:10.1016/j.pneurobio.2004.09.003 (2004).
220   9   Saper, C. B. & Lowell, B. B. The hypothalamus. *Curr Biol* **24**, R1111-1116,
221   doi:10.1016/j.cub.2014.10.023 (2014).
222   10   Wirtshafter, D., Stratford, T. R. & Shim, I. Placement in a novel environment induces fos-like
223   immunoreactivity in supramammillary cells projecting to the hippocampus and midbrain. *Brain*
224   *Res* **789**, 331-334, doi:10.1016/s0006-8993(97)01555-2 (1998).
225   11   Ito, M., Shirao, T., Doya, K. & Sekino, Y. Three-dimensional distribution of Fos-positive neurons
226   in the supramammillary nucleus of the rat exposed to novel environment. *Neurosci Res* **64**, 397-
227   402, doi:10.1016/j.neures.2009.04.013 (2009).
228   12   Kobayashi, Y. *et al.* Genetic dissection of medial habenula-interpeduncular nucleus pathway
229   function in mice. *Front Behav Neurosci* **7**, 17, doi:10.3389/fnbeh.2013.00017 (2013).
230   13   Allen Institute for Brain Science. Allen Mouse Brain Atlas. Available from: mouse.brain-
231   map.org/gene/show/12767 (2006).
232   14   Hama, H. *et al.* ScaleS: an optical clearing palette for biological imaging. *Nat Neurosci* **18**, 1518-
233   1529, doi:10.1038/nn.4107 (2015).
234   15   Soussi, R., Zhang, N., Tahtakran, S., Houser, C. R. & Esclapez, M. Heterogeneity of the
235   supramammillary-hippocampal pathways: evidence for a unique GABAergic neurotransmitter
236   phenotype and regional differences. *Eur J Neurosci* **32**, 771-785, doi:10.1111/j.1460-
237   9568.2010.07329.x (2010).
238   16   Reijmers, L. G., Perkins, B. L., Matsuo, N. & Mayford, M. Localization of a stable neural
239   correlate of associative memory. *Science* **317**, 1230-1233, doi:10.1126/science.1143839 (2007).
240   17   Hunsaker, M. R., Rosenberg, J. S. & Kesner, R. P. The role of the dentate gyrus, CA3a,b, and
241   CA3c for detecting spatial and environmental novelty. *Hippocampus* **18**, 1064-1073,
242   doi:10.1002/hipo.20464 (2008).
243   18   Pedersen, N. P. *et al.* Supramammillary glutamate neurons are a key node of the arousal system.
244   *Nat Commun* **8**, 1405, doi:10.1038/s41467-017-01004-6 (2017).
245   19   Hashimotodani, Y., Karube, F., Yanagawa, Y., Fujiyama, F. & Kano, M. Supramammillary
246   Nucleus Afferents to the Dentate Gyrus Co-release Glutamate and GABA and Potentiate Granule
247   Cell Output. *Cell Rep* **25**, 2704-2715 e2704, doi:10.1016/j.celrep.2018.11.016 (2018).
248   20   Tritsch, N. X., Granger, A. J. & Sabatini, B. L. Mechanisms and functions of GABA co-release.
249   *Nat Rev Neurosci* **17**, 139-145, doi:10.1038/nrn.2015.21 (2016).

21   Boehringer, R. *et al.* Chronic Loss of CA2 Transmission Leads to Hippocampal Hyperexcitability. *Neuron* **94**, 642-655 e649, doi:10.1016/j.neuron.2017.04.014 (2017).

22   Resendez, S. L. *et al.* Social Stimuli Induce Activation of Oxytocin Neurons Within the Paraventricular Nucleus of the Hypothalamus to Promote Social Behavior in Male Mice. *J Neurosci* **40**, 2282-2295, doi:10.1523/JNEUROSCI.1515-18.2020 (2020).

23   Wu, Z., Autry, A. E., Bergan, J. F., Watabe-Uchida, M. & Dulac, C. G. Galanin neurons in the medial preoptic area govern parental behaviour. *Nature* **509**, 325-330, doi:10.1038/nature13307 (2014).

24   Strange, B. A., Witter, M. P., Lein, E. S. & Moser, E. I. Functional organization of the hippocampal longitudinal axis. *Nat Rev Neurosci* **15**, 655-669, doi:10.1038/nrn3785 (2014).

25   Leutgeb, J. K., Leutgeb, S., Moser, M. B. & Moser, E. I. Pattern separation in the dentate gyrus and CA3 of the hippocampus. *Science* **315**, 961-966, doi:10.1126/science.1135801 (2007).

26   Senzai, Y. & Buzsaki, G. Physiological Properties and Behavioral Correlates of Hippocampal Granule Cells and Mossy Cells. *Neuron* **93**, 691-704 e695, doi:10.1016/j.neuron.2016.12.011 (2017).

27   Danielson, N. B. *et al.* Distinct Contribution of Adult-Born Hippocampal Granule Cells to Context Encoding. *Neuron* **90**, 101-112, doi:10.1016/j.neuron.2016.02.019 (2016).

28   McHugh, T. J. *et al.* Dentate gyrus NMDA receptors mediate rapid pattern separation in the hippocampal network. *Science* **317**, 94-99, doi:10.1126/science.1140263 (2007).

29   Wintzer, M. E., Boehringer, R., Polygalov, D. & McHugh, T. J. The hippocampal CA2 ensemble is sensitive to contextual change. *J Neurosci* **34**, 3056-3066, doi:10.1523/JNEUROSCI.2563-13.2014 (2014).

30   Chiang, M. C., Huang, A. J. Y., Wintzer, M. E., Ohshima, T. & McHugh, T. J. A role for CA3 in social recognition memory. *Behav Brain Res* **354**, 22-30, doi:10.1016/j.bbr.2018.01.019 (2018).

31   Hitti, F. L. & Siegelbaum, S. A. The hippocampal CA2 region is essential for social memory. *Nature* **508**, 88-92, doi:10.1038/nature13028 (2014).

32   Stevenson, E. L. & Caldwell, H. K. Lesions to the CA2 region of the hippocampus impair social memory in mice. *Eur J Neurosci* **40**, 3294-3301, doi:10.1111/ejn.12689 (2014).

33   Piskorowski, R. A. *et al.* Age-Dependent Specific Changes in Area CA2 of the Hippocampus and Social Memory Deficit in a Mouse Model of the 22q11.2 Deletion Syndrome. *Neuron* **89**, 163-176, doi:10.1016/j.neuron.2015.11.036 (2016).

34   Alexander, G. M. *et al.* Social and novel contexts modify hippocampal CA2 representations of space. *Nat Commun* **7**, 10300, doi:10.1038/ncomms10300 (2016).

35   Smith, A. S., Williams Avram, S. K., Cymerblit-Sabba, A., Song, J. & Young, W. S. Targeted activation of the hippocampal CA2 area strongly enhances social memory. *Mol Psychiatry* **21**, 1137-1144, doi:10.1038/mp.2015.189 (2016).

36   Meira, T. *et al.* A hippocampal circuit linking dorsal CA2 to ventral CA1 critical for social memory dynamics. *Nat Commun* **9**, 4163, doi:10.1038/s41467-018-06501-w (2018).

Author contributions

S.C. conceived the study and mainly conducted experiments and analyzed data under guidance and supervision of T.J.M. S.C., L.H., Y.T., A.J.H. and T.J.M performed tracing and histology. S.C., L.H., M.E.W. and A.Z.W. performed behavioral experiments. S.C. performed in vivo electrophysiology and analyzed data; R.B. and L.H. contributed to data collection; D. P. and S.J.M contributed to data analysis. T.J.M. and A.J.H. generated the mouse lines. A.J.H. produced all AAVs. V.R., L.T., V.C. and R.A.P. performed in vitro electrophysiology,

immunohistochemistry and analysis. K.N., H. Hama and A.M. performed Sca*l*e; H. Hioki provided AAV vectors for Sca*l*e. All figures were prepared by S.C. with inputs from all authors. S.C. and T.J.M. wrote the manuscript. All authors discussed the manuscript.

Data availability

Data supporting the findings of this study are available from the corresponding authors upon reasonable request.

Code availability

Custom code used in this study is available from the corresponding authors upon reasonable request.

Methods

Generation of the SuM-Cre (Csf2rb2-Cre) mouse line. The bacterial artificial chromosome (BAC) RP23-233L7 (BACPAC Resources Center) containing the colony stimulating factor 2 receptor, beta2 (*csf2rb2*) was modified using the Quick & Easy BAC Modification Kit (Gene Bridges GmbH) to insert a Cre-FRT-Amp-FRT cassette at the start site of *csf2rb2* translation. The ampicillin (Amp) marker was deleted utilizing Flp-706 recombination and the Cre-modified BAC's were confirmed by PCR analysis. The confirmed Cre-modified RP23-233L7 BAC was subsequently purified using the QIAGEN Large Construct Kit (QIAGEN). To prepare the modified BAC for microinjection, 50 µg of Cre-modified RP23-233L7 BAC was linearized using AscI (New England Biolabs (NEB)) and then buffer exchanged using the Sepharose CL-4B matrix (Pharmacia/Pfizer) into an injection buffer composed of 10 mM Tris-HCl, pH 7.4, 0.1 mM EDTA, and 100 mM NaCl. The purified BAC was injected into C57BL/6 fertilized pronuclei and fertilized blastocysts were implanted into pseudopregnant females. From the microinjections, four *Csf2rb2-Cre* B6 founders (lines 252, 267, 271, 272) were generated. The 252 *Csf2rb2-Cre* line was determined to express Cre selectively in the supramammillary area of the hypothalamus using immunohistochemistry with the anti-Cre recombinase antibody (Millipore, MAB 3120). The 252 line was maintained in a pure C57BL/6 background for all the experiments herein described and male mice between the ages of 2 and 5 months were used for all experiments.

Generation of the SuM-Cre/ Rosa-NLSLacZ mouse line. The *252 Csf2rb2-Cre* line was bred with the *Rosa-NLSLacZ*[12] line. The double transgenic *252 Csf2rb2-Cre* x *Rosa-NLSLacZ* mouse line was confirmed with PCR genotyping for both the Cre and *β*-Gal genes and designated as R252. The two lines used to generate the double transgenic line were maintained in a pure C57BL/6 background for all the experiments herein described.

Generation of the SuM-Cre/c-Fos-tTA mouse line. The 252 *Csf2rb2-Cre* line was bred with the *Tg(Fos-tTA, Fos-EGFP*)1Mmay* line (JAX 018306)[16]. The double transgenic *252 Csf2rb2-Cre* x *Tg(Fos-tTA, Fos-EGFP*)1Mmay* mouse line was confirmed with PCR genotyping for both the Cre and EGFP genes and designated as I252. The two lines used to generate the double transgenic line were maintained in a pure C57BL/6 background for all the experiments herein described and male I252 mice between the ages of 2 and 5 months were used for all experiments.

Adeno-associated viruses (AAV) vector constructions. The pAAV.EF1a.DIO.hChR2(H134R).EYFP and pAAV.EF1a.DIO.eNpHR3.0.EYFP recombinant AAV vectors were obtained from the Deisseroth Laboratory (Stanford University). The pAAV.SynTetOff.DIO.EGFP and pAAV.SynTetOff.DIO.mCherry recombinant AAV vectors were obtained from the Hioki Laboratory (Kyoto University).

The recombinant AAV vectors pAAV.EF1a.DIO.EYFP and pAAV.EF1a.DIO.mCherry were generated at our laboratory. For the construction of pAAV.EF1a.DIO.EYFP, the EYFP fragment was generated using the high fidelity Phusion DNA Polymerase (NEB). At the 5' end of the DNA fragment, the NheI restriction enzyme site is followed by the Kozak sequence and 5' ORF of the EYFP from the pAAV.DIO.hChR2(H134R).EYFP plasmid (Stanford University). The 3' end of the EYFP ORF contains the AscI restriction enzyme site. The PCR-generated cassette was digested with NheI (NEB) and AscI (NEB). The vector backbone for this construct was the pAAV.EF1a.hChR2(H134R).EYFP plasmid digested with NheI and AscI and treated with calf intestine phosphate (NEB). The approximately 5.7 kB DNA fragment containing the vector backbone was ligated to the digested EYFP ORF DNA fragment with T4 DNA ligase buffer (NEB) and transformed into One Shot Stbl3 Chemically Competent Cells (Invitrogen) and colonies were screened by restriction digest analysis. The putative positive colonies were submitted for DNA sequencing and one clone with the correct DNA sequence was designated as pAAV.EF1a.DIO.EYFP.

For the construction of pAAV.EF1a.DIO.mCherry, the mCherry fragment was generated using the high fidelity Phusion DNA Polymerase (NEB). At the 5' end of the DNA fragment, the NheI restriction enzyme site is followed by the Kozak sequence and 5' ORF of the mCherry from the pAAV.DIO.hChR2(H134R).mCherry plasmid (Stanford University). The 3' end of the mCherry ORF contains the AscI restriction enzyme site. The PCR-generated cassette was digested with

NheI (NEB) and AscI (NEB). The vector backbone for this construct was the pAAV.EF1a.hChR2(H134R).EYFP plasmid digested with NheI and AscI and treated with calf intestine phosphate (NEB). The approximately 5.7 kB DNA fragment containing the vector backbone was ligated to the digested EYFP ORF DNA fragment with T4 DNA ligase buffer (NEB) and transformed into One Shot Stbl3 Chemically Competent Cells (Invitrogen) and colonies were screened by restriction digest analysis. The putative positive colonies were submitted for DNA sequencing and one clone with the correct DNA sequence was designated as pAAV.EF1a.DIO.EYFP.

Subsequently, the recombinant AAV vector pAAV.TRE.DIO.EYFP was generated at our laboratory. For the construction of pAAV.TRE.DIO.EYFP, the TRE promoter fragment was generated by digestion of the pAAV.TRE.EYFP plasmid (previously described Chen, Weitemier, et al.) with MluI (NEB) and XbaI (NEB). The vector backbone for this construct was the pAAV.EF1a.DIO.EYFP plasmid digested with MluI and XbaI and treated with calf intestine phosphate (NEB). The approximately 4.8 kB DNA fragment containing the vector backbone was ligated to the digested TRE promoter DNA fragment with T4 DNA ligase buffer (NEB) and transformed into One Shot Stbl3 Chemically Competent Cells (Invitrogen) and colonies were screened by restriction digest analysis. The putative positive colonies were submitted for DNA sequencing and one clone with the correct DNA sequence was designated as pAAV.TRE.DIO.EYFP.

For the rabies virus experiments, the recombinant AAV vector pAAV.EF1a.DIO.TVA950 was generated at our laboratory. For the construction of pAAV.EF1a.DIO.TVA950, the EF1a promoter fragment was generated by digestion of the pAAV.EF1a.DIO.mCherry with MluI (NEB) and XbaI (NEB). The vector backbone for this construct was the pAAV.UbiquitinC.DIO.TVA950 (Johansen Laboratory, RIKEN Center for Brain Science) plasmid digested with MluI and XbaI and treated with calf intestine phosphate (NEB). The approximately 4.8 kB DNA fragment containing the vector backbone was ligated to the digested EF1a promoter DNA fragment with T4 DNA ligase buffer (NEB) and transformed into One Shot Stbl3 Chemically Competent Cells (Invitrogen) and colonies were screened by restriction digest analysis. The putative positive colonies were submitted for DNA sequencing and one clone with the correct DNA sequence was designated as pAAV.EF1a.DIO.TVA950.

14

418 Finally, the recombinant AAV vector pAAV.EF1a.DIO.H2B.GFP.2A.oG was generated at our

419 laboratory. For the construction of pAAV.EF1a.DIO.TVA950, the EF1a promoter fragment was

420 generated by digestion of the pAAV.EF1a.DIO.mCherry with MluI (NEB) and XbaI (NEB). The

421 vector backbone for this construct was the pAAV.UbiquitinC.DIO.H2B.GFP.2A.oG (Johansen

422 Laboratory, RIKEN Center for Brain Science) plasmid digested with MluI and XbaI and treated

423 with calf intestine phosphate (NEB). The approximately 7.2 kB DNA fragment containing the

424 vector backbone was ligated to the digested EF1a promoter DNA fragment with T4 DNA ligase

425 buffer (NEB) and transformed into One Shot Stbl3 Chemically Competent Cells (Invitrogen) and

426 colonies were screened by restriction digest analysis. The putative positive colonies were

427 submitted for DNA sequencing and one clone with the correct DNA sequence was designated as

428 pAAV.EF1a.DIO.H2B.GFP.2A.oG.

429 **AAV and Rabies Virus Preparation.** For adeno-associated virus production, we used the AAV

430 Helper Free System (Agilent Technologies). The adeno-associated virus vectors,

431 pAAV.DIO.EYFP, pAAV.TRE.DIO.EYFP, pAAV.DIO.hChR2(H134R).EYFP, and

432 pAAV.DIO.eNpHR3.0.EYFP were individually co-transfected with pAAV-DJ/8 (Cell Biolabs),

433 which supplies AAV2 replication proteins and AAV-DJ/8 capsid proteins, and pHelper (Agilent

434 Technologies) which supplies the necessary adenovirus gene products required for the AAV

435 production into the 293FT cell line (Invitrogen) utilizing the 293fectin transfection reagent

436 (Invitrogen). The adeno-associated virus vectors, pAAV.DIO.EYFP, AAV.DIO.mCherry,

437 pAAV.SynTetOff.DIO.EGFP, pAAV.SynTetOff.DIO.mCherry, pAAV.EF1a.DIO.TVA950 and

438 pAAV.EF1a.DIO.H2B.GFP.2A.oG were individually co-transfected with pretroAAV

439 (Addgene), which supplies AAV2 replication proteins and retrograde AAV capsid proteins, and

440 pHelper (Agilent Technologies) which supplies the necessary adenovirus gene products required

441 for the AAV production into the 293FT cell line (Invitrogen) utilizing the 293fectin transfection

442 reagent (Invitrogen). For the AAV.DJ/8 serotype AAV's, the supernatant was collected after 72

443 hours and centrifuged at 3,000 rpm for 30 minutes and then filtered through a 0.45μM filtration

444 unit (Millipore). For the retrograde serotype AAV's, the supernatant and cells were collected

445 after 72 hours and subjected to 3 cycles of freeze-thaw at −80°C and 37°C. The whole cell lysate

446 and supernatant were then centrifuged at 3,000 rpm for 30 minutes and then filtered through a

447 0.45μM filtration unit (Millipore). Subsequent purification of the DJ/8 serotype AAV and

448 retrogarde serotype AAV was carried out by ultracentrifugation (87,000 g, 4°C, 2 h) with a 20%

15

449   sucrose cushion. After ultracentrifugation, the supernatant was removed and the pellet was

450   resuspended in phosphate-buffered saline (PBS), aliquoted and stored at −80°C for long term

451   storage. The AAV stocks were titered using a custom ordered AAV stock purchased from

452   Virovek (Hayward, CA) as the reference standard. AAV titer quantification was performed using

453   qPCR with the StepOne Plus Real Time PCR System (Applied Biosystems), FastStart Universal

454   SYBR Green Master (Roche, Basel), and QPCR primers for an approximately 100 bp fragment

455   of the woodchuck hepatitis virus posttranscriptional response element (WPRE) found in all our

456   adeno-associated virus vectors. The titers for the five AAV stocks ranged between 10^{12} to 10^{13}

457   viral genome (vg)/mL for the DJ/8 serotype AAV's and between 10^{11} to 10^{12} viral genome

458   (vg)/mL for the retrograde serotype AAV's. For the pseudotyped SAD rabies virus, the

459   EnvA.RV.mCherry was generously provided by the Johansen Lab (RIKEN Center for Brain

460   Science). The titer of the EnvA.RV.mCherry rabies virus was approximately 10^9 infectious units

461   (I.U.)/mL.

462   **Stereotaxic injection and optic fiber implants.** All surgeries were performed in a stereotaxic

463   frame (Narishige). Mice were anaesthetized using 500 mg/kg Avertin. AAV's were injected

464   using a 10 μL Hamilton microsyringe (701LT, Hamilton) with a beveled 33 gauge needle

465   (NF33BL, World Precision Instruments (WPI)). A microsyringe pump (UMP3, WPI) and its

466   controller (Micro4, WPI) were used to control the speed of the injection. The needle was slowly

467   lowered to the target site and remained in place for 5 min before the beginning of the injection.

468   AAVs were typically injected at a speed of 100 nL/min. The needle was removed 10 min after

469   infusion was complete. Injections were targeted to the SuM (−2.7 mm AP, +0.4 mm ML,

470   −5.0 mm DV), bilaterally to the DG (−1.9 mm AP, +/−1.2 mm ML, −2.1 mm DV) and CA2

471   (−1.9 mm AP, +/−2.2 mm ML, −1.8 mm DV).

472   The same procedure was used for CTB injections. For the dual fluorescence tracing

473   visualization, injections of Alexa Fluor 488 CTB (1 mg/mL, 100 nL, Thermo Fisher) were

474   targeted bilaterally to the DG while the Alexa Fluor 594 CTB (1 mg/mL, 100 nL Thermo Fisher)

475   injections were targeted bilaterally to CA2.

476   For retrograde tracing of upstream inputs to the DG and CA2 projecting SuM neurons,

477   retrograde   AAV.EF1a.DIO.TVA950   and   retrograde   AAV.EF1a.DIO.H2B.GFP.2A.oG,

478   injections were targeted bilaterally to the DG or CA2. Twenty-one days post-AAV injections,

479   the EnvA.RV.mCherry SAD rabies virus was targeted to the SuM and performed as described

480   for the stereotaxic AAV injections above.

481   Optic fibers (200 μm core diameter) were bilaterally lowered above the target site (DG: −1.9 mm

482   AP, +/− 1.2 mm ML, −1.7 mm DV; CA2: −1.9 mm AP, +/− 2.2 mm ML, −1.6 mm DV). The

483   implant was secured to the skull with two jewelry screws and black opaque dental cement, which

484   also prevented light leakage from the skull.

485   **Immunohistochemistry and histology.** Mice were transcardially perfused with 4%

486   paraformaldehyde (PFA) in 0.1 M PBS (Nacalai Tesque). Brains were post-fixed in 4% PFA and

487   50 μm thick vibratome sections were prepared on a Vibratome (Leica).

488   Anti-*β*-galactosidase immunohistochemistry. After 3 x 10 min PBS washes, the sections were

489   blocked in TNB (Tris-NaCl blocking buffer) with 3% normal goat serum for 1.5 h, and incubated

490   in primary antibody (goat anti-ß-galactosidase, 1:500, Abcam) at 4°C for 20 h. After 3 x 10 min

491   washes in TNT (Tris-NaCl-Tween-20), the sections were incubated with secondary antibody

492   (goat anti-chicken IgY, Alexa Fluor 488, 1:200, Abcam) for 2 h at room temperature followed by

493   3 x 10 min washes in TNT. Fluorescence images were acquired on the Keyence BZ-X810 All-in-

494   One fluorescence microscope with either a 4x or 10x objective.

495   Anti-GFP immunohistochemistry. Anti-GFP immunohistochemistry was performed to label

496   SuM cells infected by retrograde AAV.EF1a.DIO.H2B.GFP.2A.oG injected into DG or CA2.

497   After 3 x 10 min PBS washes, the sections were blocked in TNB (Tris-NaCl blocking buffer)

498   with 3% normal donkey serum for 1.5 h, and incubated in primary antibody (goat anti-GFP,

499   1:200, Abcam) at 4°C for 20 h. After 3 × 15 min washes in TNT (Tris-NaCl-Tween-20), the

500   sections were incubated with secondary antibody (donkey anti-goat IgG, 1:200, Abcam) for 1 h

501   at room temperature followed by 3 × 15 min washes in TNT. The sections were then incubated

502   with a working solution for the TSA Plus Fluorescein Amplification Reagent (PerkinElmer) for

503   10 min at room temperature followed by 3 x 5 min washes in TNT. Fluorescence images were

504   acquired on the Keyence BZ-X810 All-in-One fluorescence microscope with either a 4x or 10x

505   objective.

506   Anti-PCP4 immunohistochemistry. After 3 x 10 min PBS rinses, the sections were blocked in

507   PBST (PBS + 0.3% Triton X-100) with 3% normal donkey serum for 1.5 h, and incubated in

17

508   primary antibody (rabbit anti-PCP4, 1:1000, Santa Cruz Biotechnologies) at 4°C for 20 h. After 3

509   x 10 min washes in PBS, the sections were incubated with secondary antibody (donkey anti-

510   rabbit, Alexa Fluor 594, 1:500, Life Technologies) for 2 h at room temperature followed by 3 x

511   10 min washes in PBS. Confocal fluorescence images were acquired on an Olympus IX81

512   confocal laser scanning microscope with a 10x or 20x objective.

513   Anti-c-Fos immunohistochemistry and histology. After 3 x 10 min PBS rinses, the sections were

514   blocked in PBST (PBS + 0.3% Triton X-100) with 3% normal donkey serum for 1.5 h, and

515   incubated in primary antibody (rabbit anti-c-Fos, 1:1000, Synaptic Systems) at 4°C for 20 h.

516   After 3 x 10 min washes in PBS, the sections were incubated with secondary antibody (donkey

517   anti-rabbit, Alexa Fluor 594, 1:500, Life Technologies) for 2 h at room temperature followed by

518   3 x 10 min washes in PBS.

519   Confocal fluorescence images were acquired on an Olympus IX81 confocal laser scanning

520   microscope with a 20x objective. To calculate the c-Fos+ cell density in Fig. 1b, three 50 μm-

521   thick sections at representative SuM coordinates (AP: -2.5, -2.8 and -3.0 mm, as shown in Fig.

522   2b) were prepared from each animal and imaged. The total number of c-Fos+ cells in the SuM

523   across the three sections was counted and divided by the total area of the SuM region to derive

524   the c-Fos+ cell density. Data from four animals was obtained for each condition (exposure to a

525   familiar context, a novel context or a novel animal) and plotted. To analyze the overlap between

526   fluorescent markers (anti-c-Fos and EYFP, mCherry and EYFP), a z-stack function was used to

527   montage 5 optical stacks (1 μm each, step size 4 μm). Filtered fluorescent images were digitally

528   combined to produce composite images and the number of cells with overlapping signals was

529   counted in the region of interest (ROI) with ImageJ. The overlap ratio in Fig. 3d was calculated

530   as (number of cells labeled in both green and red) / (total number of cells labeled in green). The

531   overlap ratio in Fig. 3j was calculated as (number of cells labeled in both green and red) /

532   (number of cells labeled in red). The overlap ratio in Extended Data Fig. 8f was calculated as

533   (number of cells labeled in both green and red) / (number of cells labeled in green). For statistics,

534   slices from at least 3 animals were obtained, imaged and analyzed. All imaging and analyses

535   were performed blind to the experimental conditions.

536   **RNAscope.** Mice were transcardially perfused with 4% PFA in 0.1 M PBS (Nacalai Tesque).

537   Brains were post-fixed in 4% PFA and 50 μm-thick vibratome sections were prepared on a

Vibratome (Leica). RNAscope hybridization was performed using the RNAscope Multiplex Fluorescent Reagent Kit v2 Assay (Advanced Cell Diagnostics). After 4 × 10 min TBS washes, free-floating slices were treated with pretreatment solutions of proprietary compositions (Advanced Cell Diagnostics). First, the slices were placed RNAscope Hydrogen Peroxide for 30 minutes at 25˚C, followed by 2 x 1 min 1x TBS washes, and 2 x 1 min 0.5x TBS washes, the slices were mounted on Superfrost Plus Slides (Fisher Scientific) were baked in a dry oven for 1 h at 60°C. The mounted slices were then placed in Target Retrieval Reagent for 15 min at 100–104°C, followed by washes in ddH$_2$O and then 100% ethanol. The slices were baked in a dry oven for 30 min at 60˚C. The slices were then placed in RNAscope Protease Plus for 30 min at 40°C followed by 2x washes in ddH$_2$O. The slices were incubated with the following trio of RNAscope probes, Mm-Slc17a6 (vGluT2), Mm-Slc32a1-C3 (vGAT), and EYFP-C2 (Advanced Cell Diagnostics) for 2 h at 40°C, followed by amplifying hybridization processes, AMP1, AMP2, and AMP3. The RNAscope probes were developed in the following order: Mm-Slc17a6 HRP-C1.Opal 570, Mm-Slc32a1-C3.Opal 690, and lastly EYFP-C2.Opal 520 (Ayoka Biosciences). The slices were counterstained with RNAscope 4',6-diamidino-2-phenylindole (DAPI) (Advanced Cell Diagnostics) for 1 min at 25°C followed by 1 – 2 drops of Prolong Gold Antifade Mountant (Thermo Fisher) before placing coverslip and sealing slides. Fluorescence images were acquired on the Keyence BZ-X810 All-in-One fluorescence microscope with either a 4x or 10x objective.

Sca*l*eS and AbSca*l*e. For selective plane illumination microscopy of whole brains, adult mice were deeply anesthetized with pentobarbital (Somnopentyl) and transcardially perfused with 4% PFA/PBS(-). The whole brain was extracted and subjected to post-fixation in 4% PFA/PBS(−) at 4°C for 24 hrs. Then, the brain samples were cleared by Sca*l*eS as described previously[23]. Observation was performed with a ZEISS Lightsheet Z.1 equipped with a 5x objective lens (Plan-Neofluor, NA = 0.16, RI = 1.45) and a 5x illumination lens (LSFM, NA = 0.1). The EYFP fluorescence was observed using a 488-nm diode laser and a 504–545 emission filter. A cleared sample was glued to the tip of a syringe (1 ml) and was positioned in front of the objective in the mounting medium (Sca*l*eS4). Images were acquired every 6.126 μm along the z-axis.

For c-Fos expression visualized by AbSca*l*e, a 0.8-mm-thick coronal brain slice was prepared from a SuM-Cre mouse infected with the Cre-dependent EYFP AAV. The EYFP fluorescent

568 images of 4%(w/v) PFA-fixed brain slices were acquired by a fluorescence stereo-microscope
569 (Leica MZ16F) equipped with a 1× objective lens (Leica PLANAPO, NA = 0.141) and a color
570 CCD camera (Zeiss AxioCam 506 color). The filters of ET-GFP (470 ± 20 nm) and ET-GFP
571 (525 ± 25 nm) were used for excitation and emission, respectively. Then, AbSca*l*e was
572 performed as described previously[14]. The brain slices were reacted with a Cy5-conjugated rabbit
573 anti-cFos polyclonal antibody (F7799, Sigma) (1.67 μg protein/mL). Multiple adjacent regions in
574 the slice were imaged with an upright laser scanning confocal microscopy system (Olympus
575 FV1200) equipped with a motorized xy stage module in addition to a motorized focus module (z-
576 drive), and a 10× dipping objective lens (Olympus XLPLN10XSVMP, NA = 0.6, WD = 6 mm,
577 RI = 1.33–1.52). The EYFP fluorescence was observed using 473 nm laser. The Cy5
578 fluorescence was observed using 635 nm laser. The adjacent regions were overlapped by 10%
579 for precise alignment. The z step size was 10 μm.

580 ***In vivo* electrophysiology.** We recorded extracellularly from SuM neurons using custom-built
581 screw-driven microdrives. The drives contain four to six independently adjustable nichrome
582 tetrodes (14 mm), gold-plated to an impedance of 200 to 250 kΩ. The relative position of each
583 tetrode exiting the cannulas on the bottom of the recording drive was mapped prior to surgery.
584 The microdrive was implanted with the tetrodes placed approximately 4.5 mm ventral from the
585 skull surface. Two days post-surgery, tetrodes were slowly lowered over several days to the
586 SuM. As the tetrode were implanted at depth, we could ensure they entered the brain smoothly
587 and perpendicularly, thus maintaining their relative positions even at their tip. During the
588 adjustment period the animal was habituated every day in a same bucket for 15 min (Familiar
589 Context) to ensure at least 10 days of habituation before the recordings started.

590 Recordings commenced once the SuM was reached based on the presence of theta oscillations
591 and high amplitude spiking. At the start of each day the tetrodes were finely adjusted to
592 maximize cell yield. Recordings started from 15-min exposure to the Familiar Context, followed
593 by 5-min exposure to a Novel Context, a second 15-min exposure to the Familiar Context and a
594 5-min exposure to a Novel Animal.

595 Neural signals and time stamps for behavior were recorded using a DigiLynx recording system
596 running Cheetah v 5.7.4 acquisition software (Neuralynx). Broadband signals from each wire
597 filtered between 0.1 and 9,000 Hz were recorded continuously at 32 kHz. The location and head

598   direction of the animal were accurately tracked by the red and green diodes affixed above the

599   animal's head.

600   After recordings were completed, mice underwent terminal anesthesia with Avertin and electrode

601   positions were marked by electrolytic lesioning of brain tissue (30 mA current for 5 s through

602   each tetrode). After transcardial perfusion with 4% PFA brains were removed and post-fixed for

603   another 24 hr in 4% PFA. Coronal slices (50 μm thick) were prepared and inspected by standard

604   light microscopy to confirm electrode placement. We cross-referenced the pattern of lesions

605   across multiple sections with the tetrode positions mapped before the implantation of the

606   recording drive to ensure precise positional assignment of each tetrode.

607   **Circuit-specific optogenetic identification and recordings.** The microdrive was fabricated in

608   the same way as described above except for the inclusion of an optic fiber with precisely

609   designed geometry to allow its placement above the CA2 or DG (DG: -1.9 mm AP, $+/-$ 1.2 mm

610   ML, -1.7 mm DV; CA2: -1.9 mm AP, $+/-$ 2.2 mm ML, -1.6 mm DV). Same procedures for

611   adjustment and recording were used, except for an additional optogenetic identification session

612   in the beginning of the recording. In this session, trains of 10 light pulses (473nm, 10 mW/mm^2)

613   were delivered to the CA2 or DG, each 20-ms long, at 10 Hz. Spike shape of the SuM neurons

614   was simultaneously measured using a broadband signal (0.1–9,000 Hz) sampled at 32 kHz.

615   Recording then continued without laser pulses as the mice explored a familiar context, a novel

616   context and a novel animal. Recording sites were later verified histologically with electrolytic

617   lesions as described above and the position of the optic fiber was also verified from the track.

618   **Data analysis.** Spikes were manually sorted with off-line software SpikeSort3D (Neuralynx).

619   The mean firing rate of each neuron was calculated using the first 5-min of data recorded in each

620   exposure condition. When two Familiar Context epochs were recorded in one recording, the

621   firing rates of each neuron in both epochs were averaged to be the mean. Putative excitatory

622   neurons (pEN) and inhibitory interneurons (pIN) were separated by the K-means clustering

623   algorithm. In addition to a threshold of meaning firing rate (neurons with firing rate <10 Hz in all

624   exposures were identified to be pEN), another two parameters, half-width of the spike and trough

625   to peak duration, were taken into account. pENs have longer trough-to-peak durations and half-

626   widths compared to pINs.

627 To determine whether a neuron's firing rate in the Novel Context or Novel Animal epoch was

628 significantly different from that in the previous Familiar Context epoch, the spike train was

629 circularly shifted by a random distance after removing the time gap between the two epochs by

630 swapping a single spike at the joint. This shuffling process was repeated 1,000 times and the

631 firing rate difference between the two shuffled epochs was calculated, to generate a P-value:

632      $P = (n+1)/(r+1)$

633 where r represents the total number of shuffles (1,000) and n is equal to the number of shuffles

634 with a firing rate difference between the two epochs greater than or equal to the unshuffled

635 value. Cells with a $P < 0.05$ were considered to have a significantly different firing rate from that

636 in the Familiar Context epoch.

637 For calculating the change of the novelty response with time, firing rates of individual neurons in

638 the three different exposures were binned in 30-s bins and normalized to the average Familiar

639 Context firing rate of all identified neurons.

640 To identify individual DG- or CA2-projecting neurons by antidromic spiking, we used a

641 combination of criteria including (a) early latency (< 20 ms from the onset of the light pulse), (b)

642 high fidelity (in response to > 50% of light pulses), and (c) mean light-evoked waveform closely

643 resembling the spontaneous waveform. Mean firing rates of the optogenetically identified cells in

644 the Familiar Context, Novel Context and Novel Animal epochs were calculated and compared.

645 **Behavioral tests and optogenetics.** For the contextual memory test, a one-day contextual

646 habituation protocol was used. Mice expressing ChR2, eNpHR or EYFP and with fibers

647 delivering light to the DG or CA2 went through six contextual exposure session: Each was 5 min

648 with 15 min intersession intervals. Mice were first placed in a novel high-walled square

649 enclosure containing 2 objects and their movement was tracked by ANY-maze (Stoelting) as

650 they explored for 5 min (Session A1). Following a 15 min intersession interval, mice were

651 returned to the same context for three additional 5 min sessions (A2, A3 and A4) with 15

652 minutes intervals in between. Only during Session A4 light (circuit activation: 473 nm, 10 Hz, 30

653 ms pulse duration, 10 mW; circuit inhibition: 532 nm, constant, 5 mW) was bilaterally delivered

654 to CA2 or DG for circuit manipulation. After a 15 minutes interval, mice were placed to a novel

655 context for 5 min exploration with light bilaterally delivered to CA2 or DG (Session B1). Again,

656 after a 15-minute interval, mice were placed back to the context for a final 5 min session in the

657 absence of light delivery (Session B2).

658 For social memory tests, a direct interaction test was used. Mice were first habituated in a

659 context for ten days (15 min per day). On the day of social familiarity test, subject mice were

660 exposed to a novel juvenile male mouse in the familiar context where the mice had been

661 habituated and allowed to interact for 5 min without light stimulation and interaction time was

662 scored. Following a 1 hour inter-trial interval the mice were re-exposed to the same juvenile

663 demonstrator, with the appropriate wavelength light (circuit activation: 473 nm, 10 Hz, 30 ms

664 pulse duration, 10 mW; circuit inhibition: 532 nm, constant, 5 mW) bilaterally delivered to CA2

665 or DG for circuit manipulation, and interaction time was scored. Habituation index was

666 calculated as (time spent exploring the familiar mouse minus time spent exploring the stimulus

667 mouse) / (time spent exploring the familiar mouse plus time spent exploring the stimulus mouse).

668 In a social novelty test, the same procedure was used except that in the second trial mice were

669 required to interact with a novel juvenile male mouse with light delivered. Habituation index was

670 calculated as (time spent exploring the novel mouse minus time spent exploring the stimulus

671 mouse) / (time spent exploring the novel mouse plus time spent exploring the stimulus mouse).

672 **In vitro electrophysiology.** For stereotaxic viral injection, animals were anaesthetized with

673 ketamine (100 mg/kg) and xylazine (7 mg/kg). The adeno-associated virus

674 AAV9.EF1a.DIO.hChR2(H134R).EYFP was used at $3x10^8$ vg/mL,

675 AAV.retro.DIO.hChR2.EYFP was used at 1.5×10^{11} vg/mL. 500 nL of virus was injected into

676 the brain of 4-week-old male csf2rb2-Cre (SuM-Cre) mice at 100 nL/min and left at the injection

677 site for 10 min following infusion. The loci of the injection sites were as follows: for medial

678 SuM, −2.8 mm anterior–posterior relative to bregma (A/P); 0 mm medial-lateral relative to

679 midline (M/L); 4.75 mm dorsal-ventral relative to surface of the brain (D/V). For CA2, -1.7 A/P,

680 1.9 mm M/L, 1.6 mm D/V. For DG, -2.0 A/P, 1.2 mm M/L, 2.1 mm D/V.

681 Transverse hippocampal slices were prepared at least 3 weeks after viral injection and whole-cell

682 patch-clamp recordings were performed from CA2 PNs and DG GCs. Animals were

683 anaesthetized with ketamine (100 mg/kg) and xylazine (7 mg/kg), and perfused transcardially

684 with a N-methyl-D-glucamin-based (NMDG) cutting solution containing the following (in mM):

685 NMDG 93, KCl 2.5, NaH_2PO_4 1.25, $NaHCO_3$ 30, HEPES 20, glucose 25, thiourea 2, Na-

686 ascorbate 5, Na-pyruvate 3, CaCl$_2$ 0.5, MgCl$_2$ 10. Brains were then rapidly removed, hippocampi

687 were dissected and placed upright into an agar mold and sliced with a vibratome (Leica

688 VT1200S) in the same cutting solution into 400 µm thick transverse slices at 4°C. Slices were

689 transferred to an immersed-type chamber and maintained in artificial cerebro-spinal fluid

690 (ACSF) containing the following (in mM) : NaCl 125, KCl 2.5, NaH$_2$PO$_4$ 1.25, NaHCO$_3$ 26,

691 glucose 10, Na-pyruvate 2, CaCl$_2$ 2, MgCl$_2$ 1. Slices were incubated at 32°C for approximately

692 20 min then maintained at room temperature for at least 45 min prior to transfer to a recording

693 chamber perfused with ACSF at 5 mL/min at 30°C. Whole-cell patch-clamp recordings were

694 performed with a cesium-based intracellular solution containing the following (in mM): Cs-

695 methyl sulfonate 130, KCl 5, EGTA-KOH 0.1, HEPES 10, NaCl 2, MgATP 5, Na$_2$GTP 0.4, Na$_2$-

696 phosphocreatine 10 and biocytin (4 mg/mL). ChR2 expressed in SuM axonal fibers was excited

697 by 488 nm light delivered by a LED attached to the epifluorescence port of the microscope.

698 Light stimulation trains consisted of 2 to10 pulses that were 0.5 ms long, delivered at 10 Hz and

699 repeated every 10–20 s for at least 20 sweeps. When blocking action potentials with TTX, light

700 pulse duration was increased to 5 ms to allow direct depolarization of pre-synaptic SuM

701 terminals (Extended Data Fig. 10). We used a light intensity of 25 mW/mm² which was

702 experimentally determined to be the minimal intensity allowing TTX-sensitive maximal

703 responses in all cell types. Data were obtained using a Multiclamp 700B amplifier, sampled at 10

704 kHz and digitized using a Digidata 1550B interface. Series resistance was < 20 MOhms and was

705 continuously monitored in voltage-clamp mode. Liquid junction potential offset of

706 approximately 10 mV was not corrected for. Pharmacological agents were added to ACSF at the

707 following concentrations (in µM): 10 NBQX and 50 D-APV to block AMPA and NMDA

708 receptors, 1 SR95531 and 2 CGP55845A to block GABAA and GABAB receptors, 100 4-

709 Aminopyridine (4-AP) to block K$_V$1 potassium channels, 0.2 TTX to prevent action potential

710 generation.

711 Midbrains containing the injection site were always examined post-hoc to ensure that infection

712 was restricted to the SuM. Post-hoc reconstruction of neuronal morphology and SuM axonal

713 projections were performed on slices and midbrain tissue following overnight incubation in 4%

714 PFA in PBS. Midbrain sections were sagitally re-sliced to 100 µm thick sections. Because

715 internal recording solutions contained Cs$^+$, we examined the cellular morphology and location of

716 all cells post-hoc to ensure data were from CA2 PNs and DG GCs (Extended Data Fig. 10).

24

Slices were permeabilized with 0.2% Triton in PBS and blocked overnight with 3% goat serum in PBS with 0.2% Triton. Primary antibody incubation was carried out in 3% goat serum in PBS overnight at 4°C. Channelrhodopsin-2 was detected by chicken primary antibody to GFP (Abcam; 1:10,000 dilution) and Alexa Fluor 488-conjugated goat-anti chicken secondary (Life Technologies, 1:300 dilution). Incubations with secondary antibodies, Alexa Fluor 594-conjugated streptavidin (Life Technologies, 1:500 dilution) and Far-red Neurotrace (Life Technologies, 1:300 dilution), were carried out in block solution for 4 hours at room temperature. After a mounting with ProlongDiamond, images were collected with a Zeiss 710 or Leica SP5 laser-scanning confocal microscope.

Electrophysiological recordings were analyzed using IGORpro (Wavemetrics) and Clampfit (Molecular devices) software. For accurate measurements of the kinetics and latencies of post-synaptic responses, the following detection process was used. For each cell, average traces were used to create a template waveform that was then fitted to individual traces and measurements were performed on the fitted trace. When only amplitudes of responses were measured, standard average peak detection was used. Results are reported ± s.e.m. Statistical significance was assessed using unpaired- or paired-Student's T test, Mann-Whitney U test, Wilcoxon signed-rank test, or Kolmogorov-Smirnoff test where appropriate.

Statistics and reproducibility. All statistical analyses were performed with GraphPad Prism 7, Excel 2010 (Microsoft) or custom MATLAB codes. The sample sizes were chosen based on common practice in similar animal experiments[7,10,11,18,19,28,29,33-36]. Experimenters were blind to genotype, region targeted and optical protocol during injections and experiments, as well as during histological and behavioral analysis. For all experiments mice were randomly assigned as to which virus they received, the injection location and protocol used. Data were first tested for normality. When normality or equal variance between samples was achieved, parametric tests such as one-way ANOVA with Turkey's post hoc test or *t*-test were used. Where normality or equal variance of samples failed, nonparametric tests such as Wilcoxon signed rank test were performed. All values were presented as mean ± s.e.m. Representative example data in all figures was selected from multiple biological replicates; Fig. 1b: 1 of 4 mice, Fig. 1f: 6 example neurons of 119 units recorded from 17 mice, Fig. 2a, b: 1 of 10 mice, Fig. 2c: 1 of 3 mice, Fig. 2d, e: 1 of 6 mice, Fig. 3c, g, i: 1 of 3 mice, Fig. 3r: 4 example neurons of 29 units recorded from 19 mice,

747 Extended Data Fig. 1b: 1 of 4 mice, Extended Data Fig. 2b: 1 of 17 mice, Extended Data Fig. 3c,

748 d: 1 of 3 mice, Extended Data Fig. 4a: 1 of 10 mice, Extended Data Fig. 4b: 1 of 3 mice,

749 Extended Data Fig. 5a, b: 1 of 3 mice, Extended Data Fig. 6a: 1 of 6 mice, Extended Data Fig.

750 6b: 1 of 3 mice, Extended Data Fig. 6e, f: 1 of 2 mice, Extended Data Fig. 7a: 1 of 6 mice,

751 Extended Data Fig. 7b: 1 of 7 mice, Extended Data Fig. 8c, e: 1 of 3 mice, Extended Data Fig.

752 8h: 1 of 8 mice, Extended Data Fig. 8k: 1 of 11 mice, Extended Data Fig. 11c, e: 1 of 4 mice,

753 Extended Data Fig. 11d, f: 1 of 5 mice.

754 **Figure 1 | SuM responds to contextual and social novelty**. **a**, Following habituation mice are
755 exposed to a novel context or a novel animal. **b**, c-Fos immunostaining in the SuM of mice after
756 exposure to a familiar context, a novel context or a novel animal. Scale bar, 200 μm. **c**,
757 Contextual and social novelty induce significant c-Fos expression in the SuM. One-way
758 ANOVA with Tukey's post hoc test, $n = 4$ mice for all groups, ****$P < 0.0001$. Open circles
759 represent values of individual mice. **d**, Behavioral recording protocol; sequential exposure to a
760 familiar context, a novel context and a novel animal. **e**, Tetrodes targeting SuM. **f**, Example
761 raster plots. Cells 1 and 2 were activated in a novel context, 3 and 4 were activated by a novel
762 animal, and 5 and 6 responded to both contextual and social novelty. FR, firing rate. **g**, Mean FR
763 of all pEN units ($n = 119$ cells from 17 mice) during novelty. One-way repeated measures
764 ANOVA with Tukey's post hoc test, *$P = 0.0240$, ****$P < 0.0001$. **h**, **i**, Scatter plots of the FRs
765 of all pEN units during novel contextual (**h**) and novel social (**i**) exposures, plotted against FRs
766 during familiar contextual exposure. Colored dots indicate neurons with significant increase in
767 FR. Pie chart summarizes fraction of population. **j**, Venn diagram of overlap between
768 subpopulations with significantly increased activity during novel contextual and novel social
769 exposures. **k**, SuM neurons with a significant FR increase after exposure to a novel context (blue,
770 $n = 26$ units) or animal (red, $n = 25$ units) displayed habituation. Black curve represents FR
771 change of the union of the above two subsets of neurons ($n = 39$ units) in a familiar context. All
772 error bars and shaded areas show mean ± s.e.m.

773

774 **Figure 2 | SuM-Cre mice reveal robust SuM-hippocampal projections**. **a**, Left: SuM
775 injection of Cre-dependent AAV in SuM-Cre mice resulted in SuM-restricted eYFP (green)
776 expression and strong terminal labeling in the DG and CA2 of the hippocampus. Right: Extent of
777 axonal terminals (eYFP, green) of SuM neurons in hippocampus along the rostrocaudal axis,
778 referenced to adapted atlas images. Scale bars, 1 mm. **b**, Cre-dependent eYFP expression in the
779 SuM of SuM-Cre mice. Numbers indicate posterior distances from bregma. Scale bars, 200 μm.
780 **c**, Left: Coronal hippocampal section showing axonal terminals of SuM neurons (eYFP, green)
781 and hippocampal neurons immunostained with anti-PCP4 (red). Scale bar, 500 μm. Right:
782 Magnified images from boxes on the left highlighting SuM axons targeting granule cells in the
783 DG and pyramidal neurons in CA2, both PCP4 positive (red). Scale bars, 50 μm. **d**, **e**, Bilateral

injection of retroAAV-DIO-mCherry to hippocampal DG and retroAAV-DIO-EYFP to CA2 of the SuM-Cre mice selectively labels DG-projecting SuM neurons with mCherry and CA2-projecting SuM neurons with eYFP. Axons targeting the hippocampus are shown in **d** (scale bar, 500 μm), and soma in the SuM are shown in **e** (scale bars, 200 μm). Numbers in **e** indicate posterior distances from bregma.

Figure 3 | DG- and CA2-projecting SuM neurons respond to contextual and social novelty, respectively. **a**, Experimental design to examine the overlapping SuM populations that respond to two novelty exposures. **b**, Double transgenic mice (SuM-Cre/c-Fos-tTA) were injected with AAV-TRE-DIO-EYFP. **c**, Images of overlapping populations in the SuM activated by two novelty exposures. On the right of each image is a magnified view of the area within the white box (200 × 200 μm). **d**, eYFP+/c-Fos+ overlap SuM cell counts for the conditions shown in **c**. One-way ANOVA with Tukey's post hoc test, $n = 3$ mice for all groups, ****$P < 0.0001$. **e**, Protocol to examine the projection specificity of SuM populations that respond to novel contextual or social exposure. **f**, **h**, Strategy to simultaneously label DG- (**f**) or CA2- (**h**) projecting SuM cells using retroAAV-DIO-mCherry and novelty-responsive cells using AAV-TRE-DIO-EYFP with the SuM-Cre/c-Fos-tTA mice. **g**, **i**, Images of overlapping populations in the SuM that were activated by contextual or social novelty and projected to the DG or CA2. On the right of each image is a magnified view of the area within the white box (200 × 200 μm). **j**, eYFP+/mCherry+ overlap SuM cell counts for the conditions shown in **g** and **i**. One-way ANOVA with Tukey's post hoc test, $n = 3$ mice for all groups, ***$P = 0.0004$, ****$P < 0.0001$. **k**, Protocol for a recording session to optogenetically identify DG- or CA2-projecting SuM neurons. **l**, **o**, Viral injection, optic fiber and tetrodes implantation. **m**, **p**, Peristimulus time histograms of representative single units photoidentified as SuM-DG (**m**) and SuM-CA2 (**p**) projectors. **n**, **q**, Waveforms of spontaneous (grey) and light-evoked antidromic (blue) spikes of the single units in **n** and **q**. **r**, Raster plots of sample neurons. Cells 1 and 2 projecting to DG were more active in a novel context, and Cells 3 and 4 projecting to CA2 preferentially responded to a novel animal. FR, firing rate. **s**, **t**, Calculated FR changes of DG-projecting (**s**, $n = 12$ putative excitatory neurons from 8 mice, **$P = 0.0024$) and CA2-projecting (**t**, $n = 17$ putative excitatory neurons from 11 mice, ***$P = 0.0003$) SuM neurons in response to

814   contextual and social novelty. FR change = (FR in Contextual or Social minus FR in Familiar) /

815   (FR in Contextual or Social plus FR in Familiar). Two-tailed Wilcoxon matched-pairs signed

816   rank test. All error bars show mean ± s.e.m. Open circles are values from individual mice. Scale

817   bars, 200 μm.

818

819   **Figure 4 | SuM-hippocampal circuits selectively modulate contextual and social memory. a**,

820   Protocol used for contextual memory tests. **b–e**, Distance traveled during each contextual

821   exposure normalized to Session A1 under optogenetic manipulations of SuM-hippocampal

822   circuits. Light was delivered in Sessions A4 and B1 to the DG or CA2. Two-way ANOVA with

823   Bonferroni post hoc test, $n = 11$ mice (DG/ChR2) versus $n = 11$ (DG/eYFP) in **b** (*$P = 0.0119$, F

824    $(20, 100) = 2.961$), $n = 11$ (DG/eNpHR) versus $n = 9$ (DG/eYFP) in **c** (****$P < 0.0001$, F (18,

825    $90) = 3.490$), $n = 11$ (CA2/ChR2) versus $n = 9$ (CA2/eYFP) in **d**, $n = 10$ (CA2/eNpHR) versus n

826    $= 12$ (CA2/eYFP) in **e**. **f**, Protocol used for social familiarity tests. **g**, **h**, Habituation index with a

827   familiar animal under various optogenetic manipulations of SuM-hippocampal circuits. Two-

828   tailed unpaired t-tests, $n = 13$ mice (DG/ChR2) versus $n = 9$ (DG/eYFP), $n = 10$ (DG/eNpHR)

829   versus $n = 11$ (DG/eYFP) in **g**, $n = 17$ (CA2/ChR2) versus $n = 19$ (CA2/eYFP), $n = 10$

830   (CA2/eNpHR) versus $n = 13$ (CA2/eYFP) in **h**, ***$P = 0.0008$, t (34) = 3.665. **i**, Protocol used

831   for social novelty tests. **j**, **k**, Habituation index with a novel animal under various optogenetic

832   manipulations of SuM-hippocampal circuits. Two-tailed unpaired t-tests, $n = 13$ mice

833   (DG/ChR2) versus $n = 9$ (DG/eYFP), $n = 10$ (DG/eNpHR) versus $n = 11$ (DG/eYFP) in **j**, $n = 13$

834   (CA2/ChR2) versus $n = 10$ (CA2/eYFP), $n = 16$ (CA2/eNpHR) versus $n = 12$ (CA2/eYFP) in **k**.

835   n.s., nonsignificant. Error bars show mean ± s.e.m. Boxes denote median (centre line), 25th and

836   75th percentiles (box edges), and full range of values (whiskers).

837

838   **Extended Data Figure 1 | Identification of hypothalamic regions activated by contextual**

839   **and social novelty**. **a**, Counts of c-Fos+ cells in hypothalamic regions that show response to

840   contextual and social novelty. *$P = 0.0140$, **$P = 0.0023$, ***$P = 0.0009$, ****$P < 0.0001$. n.s.,

841   nonsignificant. Two-way ANOVA with Tukey's post hoc test, $n = 4$ mice for all groups. Error

842   bars indicate mean ± s.e.m. Open circles are values from individual mice. **b**, Example c-Fos

843   immunostaining (red) in the hypothalamus of one mouse from a total of 4 replicates at various

844 distances from bregma along the rostrocaudal axis of mice 1.5 h after exposure to a familiar

845 context, a novel context or a novel animal. AHN, anterior hypothalamic nucleus; DMH, dorsal

846 medial hypothalamic nucleus; LHA, lateral hypothalamic area; LPO, lateral preoptic area; MM,

847 medial mammillary nucleus; MPN, medial preoptic nucleus; MPO, medial preoptic area; PH,

848 posterior hypothalamic nucleus; PVH, paraventricular hypothalamic nucleus; SuM,

849 supramammillary nucleus; VMH, ventromedial hypothalamic nucleus. Scale bars, 500 μm.

850

851 **Extended Data Figure 2 | Histology of recorded animals and firing rate analysis of**

852 **interneurons. a**, Tetrode recordings in the SuM. **b**, An example coronal section of the SuM from

853 one of 17 mice used for recording with tetrode locations indicated by arrows. Scale bar, 400 μm.

854 **c**, Reconstructed tetrode tip locations (71 in target and 14 off target) from 17 animals overlaid

855 onto schematic mouse brain slices. Numbers indicate posterior distances from bregma. **d**,

856 Behavioral protocol for a recording session, including sequential exposure to a familiar context,

857 a novel context and a novel animal. **e**, Mean FR of all pIN (putative interneuron, $n = 22$ from 17

858 mice) units during different exposures. FR, firing rate. One-way repeated measures ANOVA.

859 n.s., nonsignificant. **f**, **g**, Scatter plots of the FRs of all IN units during novel contextual (**f**) and

860 novel social (**g**) exposures, plotted against FRs during familiar contextual exposure. Colored dots

861 indicate interneurons that showed a significant increase in FR. Horizontal and vertical green bars

862 indicate 10 Hz, the low threshold of FR to classify interneurons. Pie graphs show the percentage

863 of pIN units that exhibited significant increase, significant decrease, or no change in FR during

864 the respective novelty exposure. **h**, Venn diagram of overlap between subpopulations with

865 significantly increased activity during novel contextual and novel social exposures.

866

Extended Data Figure 3 | Generation and characterization of the SuM-Cre mouse line. a, Recombination strategy for SuM-specific expression of Cre recombinase driven by the csf2rb2 promoter. Diagram shows the schematic of the csf2rb2 promoter.Cre.FRT.AmpR.FRT construct. **b**, Example anti-Cre immunostaining in the SuM of the SuM-Cre mouse (one of three replicates). Dotted white line indicates the anatomical boundary of the SuM. Scale bar, 500 μm. **c**, **d**, Coronal (**c**) and sagittal (**d**) sections (scale bars, 2 mm) prepared from an adult progeny (age 12 weeks) of SuM-Cre and Rosa-NLSLacZ crosses and immunostained with anti-*ß*-galactosidase (*ß*-gal, recombination marker). Representative images of from all brain regions where recombination is identified are shown from one mouse of four replicates of each. Dotted white lines indicate the boundaries of these brain regions. On the right of each image in **c** is a magnified view of the area within the white box (scale bars, 1 mm). BLA, basolateral amygdala; LHA, lateral hypothalamic area; PAG, periaqueductal gray; PF, parafascicular thalamic nucleus; PH, posterior hypothalamic nucleus; RL, rostral linear nucleus raphe; SuM, supramammillary nucleus. Scale bars, 2 mm.

Extended Data Figure 4 | Brain-wide mapping of projections from SuM neurons. a, Coronal sections prepared from a SuM-Cre mouse injected with AAV-DIO-EYFP into the SuM. AcbSh, accumbens nucleus, shell; AHN, anterior hypothalamic nucleus; CM, central medial thalamic nucleus; DG, dentate gyrus; DP, dorsal peduncular cortex; fi, fimbria of hippocampus; IAM, interanteromedial thalamic nucleus; IG, induseum griseum; LHA, lateral hypothalamic area; LHb, lateral habenular nucleus; LPO, lateral preoptic area; LS, lateral septal nucleus; MD, mediodorsal thalamic nucleus; MDl, mediodorsal thalamic nucleus, lateral part; MPO, medial preoptic area; MS, medial septal nucleus; PH, posterior hypothalamic nucleus; RE, nucleus of reuniens; SFi, septofimbrial nucleus; SHi, septohippocampal nucleus; SuM, supramammillary nucleus; vhc, ventral hippocampal commissure. Example is one mouse of four replicates. **b,** Sagittal sections prepared from a SuM-Cre mouse injected with AAV-DIO-EYFP into the SuM. Example shown is one mouse of 3 replicates. Scale bars, 500 μm.

Extended Data Figure 5 | Examination of projections (a) and activity (b) of SuM neurons by clearing and rapid 3D imaging with light sheet microscopy using the Sca*l*eS method. a,

897 Whole-brain examination of SuM projections. AAV-DIO-EYFP was injected to the SuM of

898 SuM-Cre mice to label SuM projections by Cre-dependent EYFP expression. Acb, accumbens

899 nucleus; DG, dentate gyrus; EC, entorhinal cortex; SuM, supramammillary nucleus. Scales: 14.6

900 mm (x) × 17.1 mm (y) × 7.5 mm (z) for horizontal views and 11.7 mm (x) × 17.6 mm (y) × 9.0

901 mm (z) for the sagittal view. One example of 3 replicates is shown. **b**, AbSca*l*e shows EYFP+/c-

902 Fos+ neurons in the SuM after exposure to contextual (left, Mouse #252-1263) or social novelty

903 (right, Mouse #252-1265). 800 μm thick coronal slices were cleared and c-Fos was stained by

904 AbSca*l*e, followed by rapid 3D imaging with laser-scanning confocal microscopy. One example

905 of 3 replicates is shown. Scale bars in the top panel, 1 cm. Scale bars in other panels, 500 μm.

906

907 **Extended Data Figure 6 | Retrograde tracing of SuM neurons projecting to DG and CA2. a**,

908 Collateral projections of DG and CA2-projecting SuM neurons. Dual-color Cre-dependent

909 retrograde AAVs were used to label the cell bodies and axons of SuM neurons projecting to DG

910 (mCherry, red) and CA2 (EYFP, green) (see also Fig. 2d, e). Weak collateral projections from

911 DG and CA2-projecting SuM neurons could be seen in the medial (MS) and lateral septal

912 nucleus (LS) and lateral hypothalamic area (LHA). One example of 6 replicates is shown. Scale

913 bars, 500 μm. **b**, Dual-color cholera toxin subunit B (CTB) labeling was used to trace the cell

914 bodies of SuM neurons projecting to DG (CTB 488, green) and CA2 (CTB 594, red). The

915 majority of the identified SuM cell bodies were found to project solely either to the DG or CA2

916 with only 2.6 ± 0.5% (N = 3 mice, n = 708 neurons) projecting to both. Scale bars, 250 μm. **c**, **d**,

917 Strategy for multiplex fluorescent in situ hybridization (RNAscope) to identify VGLUT2 and

918 VGAT mRNAs present in the cell bodies of DG- and CA2-projecting SuM neurons. Cre-

919 dependent retrograde AAV was used to label the cell bodies and axons of SuM neurons

920 projecting to DG (**c**) and CA2 (**d**). **e**, **f**, DG- (**e**) and CA2-projecting (**f**) SuM neurons were

921 stained by antisense probes directed against VGLUT2 (570 nm), VGAT (690 nm), and EYFP

922 (520 nm) mRNAs. Scale bars, 500 μm. **g**, **h**, Quantification of EYFP+/VGLUT2+/VGAT+ and

923 EYFP+/VGLUT2+/VGAT- neurons in the DG- (**g**) and CA2-projecting (**h**) SuM neurons. n = 2

924 animals for each group. All the DG-projecting and CA2-projecting neurons are VGLUT2+. The

925 majority (average: 71.3%, Animal 1: 72.2%, Animal 2: 70.3%) of DG-projecting neurons are

926 VGAT+, while only a small portion (average: 13.1%, Animal 1: 12.3%, Animal 2: 13.8%) of
927 CA2-projecting neurons are VGAT+.

928

929 **Extended Data Figure 7 | Validation of the functional segregation of SuM-DG and SuM-**
930 **CA2 circuits. a**, **b**, Strategies of whole-cell voltage clamp recording experiments to validate the
931 physiological segregation of SuM-DG and SuM-CA2 circuits. Retrograde AAV-DIO-ChR2-
932 EYFP was bilaterally injected into the DG (**a**) or CA2 (**b**) of SuM-Cre mice to infect DG- (**a**) or
933 CA2-projecting (**b**) SuM cells. Two weeks later, acute transverse hippocampal slices were
934 prepared and whole-cell voltage clamp recordings were performed in CA2 pyramidal neurons
935 (PNs, **a**) or DG granule cells (GCs, **b**) in order to determine if the DG-projecting SuM neurons
936 also innervated CA2 cells (**a**), and vice versa (**b**). All recorded cells were filled with biocytin for
937 post-hoc identification. Lower panels are confocal images of transverse hippocampal slices
938 recorded with Nissl (blue), ChR2-EYFP expressing SuM fibers (green), and biocytin-filled (red)
939 CA2 PN (**a**) or DG GC (**b**). Scale bars, 250 μm. **c**, **d**, Example light-evoked IPSCs (10 traces,
940 light red; average trace, red) and light-evoked EPSCs (10 traces, grey; average trace, black)
941 recorded with 5 light pulses in CA2 PNs (**c**) and DG GCs (**d**). No inhibitory or excitatory light-
942 evoked current was detected for any of the 17 CA2 PNs from 6 mice and 19 DG GCs from 7
943 mice, suggesting that DG-projecting SuM cells do not innervate CA2, and vice versa. **e**, **f**,
944 Strategies of behavioral experiments to examine the effect from light bleed-through on the
945 optogenetic dissection of SuM-DG and SuM-CA2 circuits. RetroAAV-DIO-ChR2 was
946 bilaterally injected into the DG (**e**) or CA2 (**f**) of SuM-Cre mice to infect DG- (**e**) or CA2-
947 projecting (**f**) SuM cells. Optic fiber was bilaterally implanted in the uninjected region of each
948 mouse: DG-ChR2 with fibers in CA2 (**e**) or CA2-ChR2 with fibers in DG (**f**). **g–j**, Contextual (**g**,
949 **h**) and social (**i**, **j**) memory tests. Light was delivered to the uninfected region of the
950 hippocampus: DG-ChR2 with light delivery to CA2 (**g**, **i**) or CA2-ChR2 with light delivery to
951 DG (**h**, **j**). Two-way ANOVA with Bonferroni post hoc test, $n = 8$ mice (DG/ChR2) versus $n = 8$
952 (DG/eYFP) in **g**, $n = 8$ mice (CA2/ChR2) versus $n = 8$ (CA2/eYFP) in **h**. Two-tailed unpaired *t*-
953 tests, $n = 8$ mice (DG/ChR2) versus $n = 8$ (DG/eYFP) in **i**, $n = 8$ mice (CA2/ChR2) versus $n = 8$
954 (CA2/eYFP) in **j**. n.s., nonsignificant. Error bars show mean ± s.e.m. Boxes denote median
955 (centre line), 25th and 75th percentiles (box edges), and full range of values (whiskers).

33

956

957

Extended Data Figure 8 | Circuit-specific c-Fos mapping and optogenetic identification and recording. **a**, Experimental design to examine the projection specificity of SuM populations that respond to novel contextual or novel social exposure. **b**, **d**, Strategy to label DG- (**b**) or CA2- (**d**) projecting SuM cells using retroAAV-DIO-EYFP with the SuM-Cre mice. **c**, **e**, Images of overlapping populations in the SuM that had contextual or social novelty-induced c-Fos expression and projected to the DG or CA2. On the right of each image is a magnified view of the area within the white box (200 × 200 μm). One example of 3 replicates is shown. **f**, EYFP+/c-Fos+ overlap SuM cell counts for the conditions shown in **c** and **e**. DG-projecting SuM neurons were preferentially activated by contextual novelty (DG-projecting: $53.3 \pm 6.1\%$ versus CA2-projecting: $37.1 \pm 0.4\%$, *$P = 0.0429$, one-way ANOVA with Tukey's post hoc test, $n = 3$ mice for both groups), whereas CA2-projecting neurons responded more to social novelty (CA2-projecting: $50.2 \pm 1.8\%$ versus DG-projecting: $25.4 \pm 2.7\%$, **$P = 0.0042$, one-way ANOVA with Tukey's post hoc test, $n = 3$ mice for both groups). All error bars show mean ± s.e.m. Open circles are values from individual mice. Scale bars, 200 μm. **g**, **j**, Strategies for optogenetic identification and recording DG- (**g**) and CA2-projecting (**j**) neurons in the SuM. **h**, **k**, Example coronal sections of the SuM with tetrode locations indicated by arrows. Scale bars, 200 μm. **i**, **l**, Histology of recorded animals for circuit-specific optogenetic identification and recording. Reconstructed tetrode tip locations overlaid onto schematic mouse brain slices are shown. Numbers indicate posterior distances from bregma. 35 tetrodes were in target and 8 out of target from 8 mice for recording DG-projecting neurons, while 49 tetrodes were in target and 9 out of target from 11 mice for recording CA2-projecting neurons.

979

Extended Data Figure 9 | Behavioral tests for contextual memory. a, Familiar (A1-A4 in **b**) and novel contexts (B1 and B2 in **b**) used for contextual memory tests. **b**, Behavioral protocol. **c–e**, Example traveling trajectories of animals during each contextual exposure described in **b** under different optogenetic manipulations of the SuM-DG circuit. **f–i**, Percentage of distances traveled during each contextual exposure under various optogenetic manipulations. Light was delivered in Sessions A4 and B1 to the DG or CA2. The no-light data were used as the control,

34

in supplementary to the EYFP controls in Fig. 4b–e. Two-way ANOVA with Bonferroni post hoc test, $n = 11$ mice (DG/ChR2/light) versus $n = 11$ (DG/ChR2/no light) in **f** (**$P = 0.0013$, $F_{(20, 100)} = 2.882$), $n = 11$ (DG/eNpHR/light) versus $n = 11$ (DG/eNpHR/no light) in **g** (****$P < 0.0001$, $F_{(20, 100)} = 2.402$), $n = 11$ (CA2/ChR2/light) versus $n = 11$ (CA2/ChR2/no light) in **h**, $n = 10$ (CA2/eNpHR/light) versus $n = 10$ (CA2/eNpHR/no light) in **i**. All error bars show mean ± s.e.m.

Extended Data Figure 10 | Synaptic transmission from SuM terminals to DG granule cells (GCs) and CA2 pyramidal neurons (PNs). **a**, Identification of direct glutamatergic transmission in CA2 from SuM inputs. (left) Diagram illustrating the whole-cell recordings of hippocampal pyramidal neurons (PNs) and SuM fiber stimulation in acute slice preparation. Cesium-based intracellular solution was used in the recording pipette and all cells were recorded in voltage-clamp mode with a membrane potential held at -70 mV in order to record excitatory glutamatergic transmission. (right) Diagram mapping the location of all PNs recorded in the hippocampus with closed circles indicating connected cells and open circles indicating unconnected cells with no detected transmission. Cells were classified as CA1 ($n = 11$, all unconnected), CA2 ($n = 46$ connected, $n = 30$ unconnected) and CA3 ($n = 19$ connected, $n = 29$ unconnected) based on morphology (the presence of thorny excrecsences for CA3) and location. Circle color indicates cell type with CA2 PNs black, CA3 PNs brown and CA1 PNs orange. **b**, Identification of feed-forward inhibitory transmission in CA2 from SuM inputs. (left) Diagram illustrating the local circuitry involved in the feed-forward inhibition recruited by SuM inputs in the hippocampus. The same recording configuration was used as shown in **a**, except that cells were held at +10 mV in order to measure feed-forward inhibitory transmission. (right) Diagram mapping PNs in the hippocampus that receive feed-forward transmission from light-evoked SuM inputs with unconnected cells shown as open circles and connected cells as filled circles. No CA1 PNs received feed-forward inhibition ($n = 11$) while over half of CA2 PNs received detectable feed-forward inhibition ($n = 30$ connected, $n = 18$ unconnected) as well as a fraction of CA3 PNs ($n = 20$ connected, $n = 18$ unconnected). **c**, Identification of excitatory and inhibitory transmission to DG granule cells (GCs) from SuM inputs. (left) Diagram illustrating the experimental setup to measure local excitatory and inhibitory circuitry recruited by SuM

1016   inputs in the DG. The same recording configuration was used as shown in **a** and **b**. Cells were
1017   held at -70 mV to measure excitatory transmission and then at +10 mV. Inhibitory transmission
1018   was measured before and after the addition of 10 µM NBQX & 50 µM APV to distinguish feed-
1019   forward and direct inhibitory transmission. (right) Diagram mapping GCs in the DG that receive
1020   excitatory and inhibitory (both feed-forward and direct) transmission from light-evoked SuM
1021   inputs. Blue filled circles mark the location of cells that received both excitatory and inhibitory
1022   transmission (n = 21). All cells received both direct and feed-forward inhibition. Yellow-filled
1023   circles mark cells that did not receive detectable excitatory transmission, but both direct and
1024   feed-forward inhibitory transmission (n = 3). Data for panels **a.-c.** were collected from 156
1025   slices from 92 mice. Abbreviations: so, stratum oriens; sp, stratum pyramidale; sr, stratum
1026   radiatum; mf, mossy fiber; ml, molecular layer; gcl, granule cell layer. **d**, Inverted epifluorescent
1027   image of a hippocampal slice with a DG GC and a CA2 PN. Each neuron had been recorded and
1028   filled with biocytin which was stained with streptavidin-conjugated fluorophore. **e**, Dendritic
1029   (blue) and axonal (red) reconstruction of the cells in **d** with the hippocampal regions demarcated.
1030   **f**, Diagram illustrating the local circuitry and whole-cell recording configuration of DG GCs in
1031   acute brain slices prepared from SuM-Cre mice injected with AAV-DIO-ChR2-EYFP. SuM
1032   axonal terminals were illuminated by a 0.5 ms 488 nm light stimulation. IN, interneuron. **g**,
1033   Sample traces of light-evoked EPSCs recorded at −70 mV (individual traces in grey, average
1034   trace in black) and IPSCs recorded at +10 mV (individual traces in light red, average trace in red)
1035   in a same DG GC under voltage clamp. The blue line denotes when the light stimulus was
1036   applied. **h**, Normalized cumulative distribution of latencies for DG GC EPSCs (black) and IPSCs
1037   (red), both displaying response latencies consistent with direct monosynaptic transmission (4.1 ±
1038   0.3 ms for EPSCs, n = 20 GCs; 4.16 ± 0.3 ms for IPSCs, n = 22 GCs; Student's t-test, P = 0.94;
1039   Kolmogorov–Smirnov test, P = 0.97). **i**, **j**, Sample traces (**i**) and time course of amplitudes (**j**,
1040   IPSCs only, n = 22 GCs from 8 mice) of light-evoked EPSCs (black) and IPSCs (red) recorded
1041   in DG GCs before and after application of 10 µM NBQX & 50 µM APV (grey), and further
1042   application of 1 µM SR95531 & 2 µM CGP55845A (green). AMPA and NMDA receptor
1043   blockers completely blocked EPSCs (13 ± 3.1 pA, n = 20 GCs), but only partially blocked IPSCs
1044   (by 36%, 86 ± 21 pA before, 31 ± 7.2 pA following NBQX and APV addition, **P =0.0037**,
1045   Wilcoxon signed-rank test, n = 22 GCs from 8 mice), indicating that there is feed-forward
1046   inhibition recruited by SuM inputs, accompanied by a larger amount of direct inhibitory

transmission. The remaining light-evoked IPSCs were entirely blocked by the subsequent addition of GABAA and GABAB receptor blockers, suggesting that DG-projecting neurons in the SuM are capable of simultaneously releasing both glutamate and GABA. **k**, Diagram similar to **f**, showing the local circuitry and whole-cell recording configuration of CA2 PNs. **l**, Sample traces of EPSCs recorded at −70 mV (individual traces in grey, average trace in black) and IPSCs recorded at +10 mV (individual traces in light red, average trace in red) in a same CA2 PN under voltage clamp. Note the increased latency of IPSCs onset compared to EPSCs. **m**, Normalized cumulative distribution of latencies for CA2 PN EPSCs (black) and IPSCs (red). IPSCs displayed significantly different response latencies from the EPSCs, with a longer IPSC response latency consistent with bi-synaptic feed-forward inhibition (2.9 ± 0.1 ms for EPSCs, $n = 166$ PNs; 6.2 ± 0.4 ms for IPSCs, $n = 69$ PNs; ****$P < 0.0001$, Mann–Whitney U test; Kolmogorov–Smirnov test, ****$P < 0.0001$, data from 92 mice). **n**, **o**, Sample traces (**n**) and time course of amplitudes (**o**, IPSCs only, $n = 7$ from 4 mice) of light-evoked EPSCs (black) and IPSCs (red) recorded in CA2 PNs before and after application of 10 μM NBQX & 50 μM APV (grey). Both the EPSCs (16 ± 4.8 pA, $n = 6$ PNs from 4 mice) and IPSCs (167 ± 40 pA, $n = 7$ PNs from 4 mice) were completely blocked by the application of AMPA and NMDA receptor blockers, indicating that the synaptic transmission from the SuM is entirely glutamatergic in CA2. Notably, both SuM-DG and SuM-CA2 transmissions recruit a robust feed-forward inhibition. **p**, Confirmation of SuM-CA2 transmission by the addition of tetrodotoxin (TTX) and 4-aminopyridine (4-AP) to isolate transmitter release resulting from direct optical terminal depolarization. Application of TTX & 4-AP abolishes IPSCs and spares EPSCs in CA2 pyramidal neurons (PNs), consistent with mono-synaptic excitation and di-synaptic inhibition. Control sample traces are shown in black (EPSC) and red (IPSC), while traces following application of TTX & 4-AP are shown in grey. **q**, Time course of light-evoked EPSC and IPSC amplitudes upon application of 0.2 μM TTX & 100 μM 4-AP in which a longer light stimulus was used to directly depolarize the SuM axonal terminal. Initial amplitudes were 20.2 ± 6.1 pA for EPSCs and 110 ± 50 pA for IPSCs, and 9.3 ± 7.7 pA for EPSCs and 4.8 ± 0.7 pA for IPSCs following TTX & 4-AP, indicating a 61 ± 24 % block of EPSCs and 88 ± 4.2 % block of IPSCs by TTX & 4-AP. $P = 0.22$ for EPSCs, $P = 0.016$ for IPSCs, Wilcoxon signed-rank test, $n = 7$ PNs from 3 mice. All error bars show mean ± s.e.m.
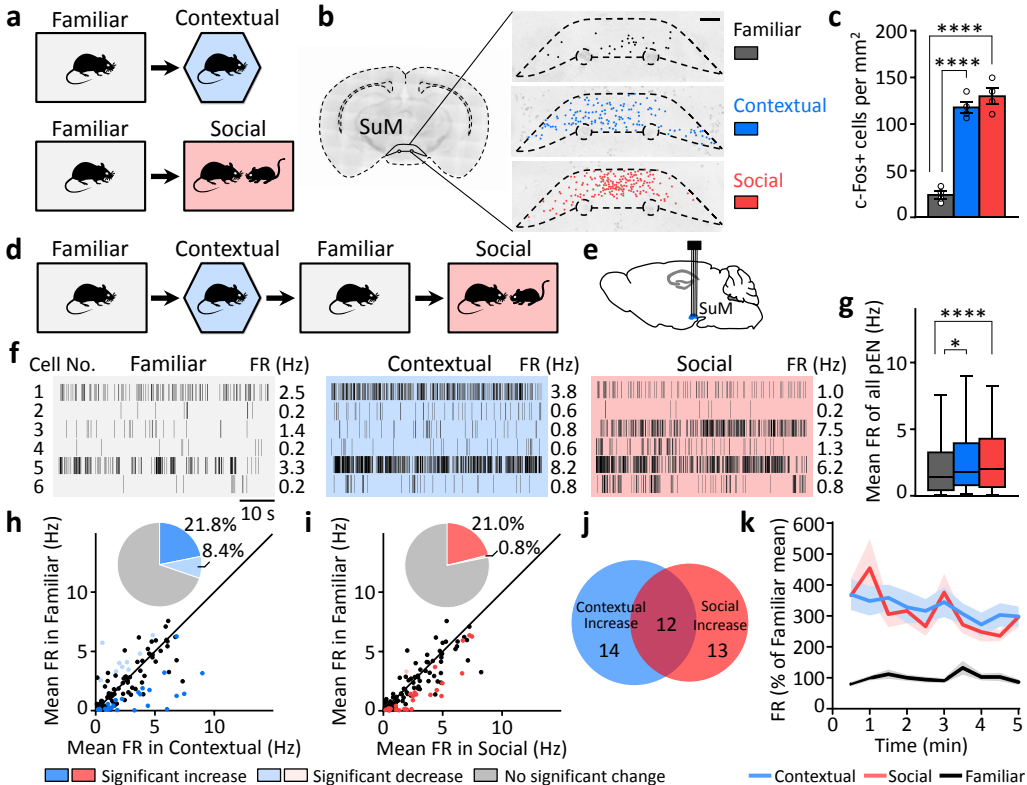
Extended Data Figure 11 | Retrograde tracing of upstream inputs to the DG- and CA2-projecting SuM neurons. a, **b**, Strategies of projection-specific retrograde tracing to map the upstream inputs to the DG- (**a**) and CA2-projecting (**b**) neurons. Retrograde AAV helper viruses expressing the rabies G protein and the TVA receptor are injected into DG (**a**) or into CA2 (**b**), and three weeks later EnvA pseudotyped rabies virus expressing mCherry is injected into the SuM. This allows for the retrograde labeling of upstream neurons that send efferent axons to DG- or CA2-projecting SuM cells by the rabies virus. **c**, **d**, Coronal sections showing DG- (**c**) and CA2-projecting (**d**) starter cells in the SuM. Cells in red (mCherry) are TVA+ cells that express rabies virus (one example of four mice for DG injections, one example of five mice for CA2 injections). Cells in green (GFP) express oG (optimized glycoprotein). The mCherry+/GFP+ overlapping cells (yellow) are starter cells where the *trans*-complementation of RV*dG* with oG results in the production of oG+RV*dG* that spreads trans-synaptically to input cells. Scale bar, 1 mm. **e**, **f**, Coronal sections with trans-synaptically labeled input cells upstream to the DG- (**e**) and CA2-projecting (**f**) SuM neurons. Scale bars, 1 mm. **g**, **h**, Quantification of inputs from various brain regions to the DG- (**g**, $n = 4$ mice) and CA2-projecting (**h**, $n = 5$ mice) SuM neurons. Both populations received extensive inputs from subcortical regions including the hypothalamus, brainstem, septum and nucleus accumbens. However, the inputs to the DG-projecting population were comparatively biased to brain regions in the reward and motor systems, such as the VTA, SI, AcbSh, LS and MS, while the CA2 projectors received proportionally greater inputs from neurons in socially engaged regions, particularly the PVH (*$P = 0.0159$, Mann-Whitney U test) and MPO. All error bars show mean ± s.e.m. LS, lateral septal nucleus; MS, medial septal nucleus; SI, substantia innominata; AcbSh, accumbens nucleus, shell; ZI, zona incerta; LHA, lateral hypothalamic area; MPO, medial preoptic area; LPO, lateral preoptic area; PVH, paraventricular hypothalamic nucleus; PH, posterior hypothalamic nucleus; PAG, periaqueductal gray; MRN, midbrain reticular nucleus; VTA, ventral tegmental area; Raphe: DR, dorsal raphe nucleus & MnR, median raphe nucleus.
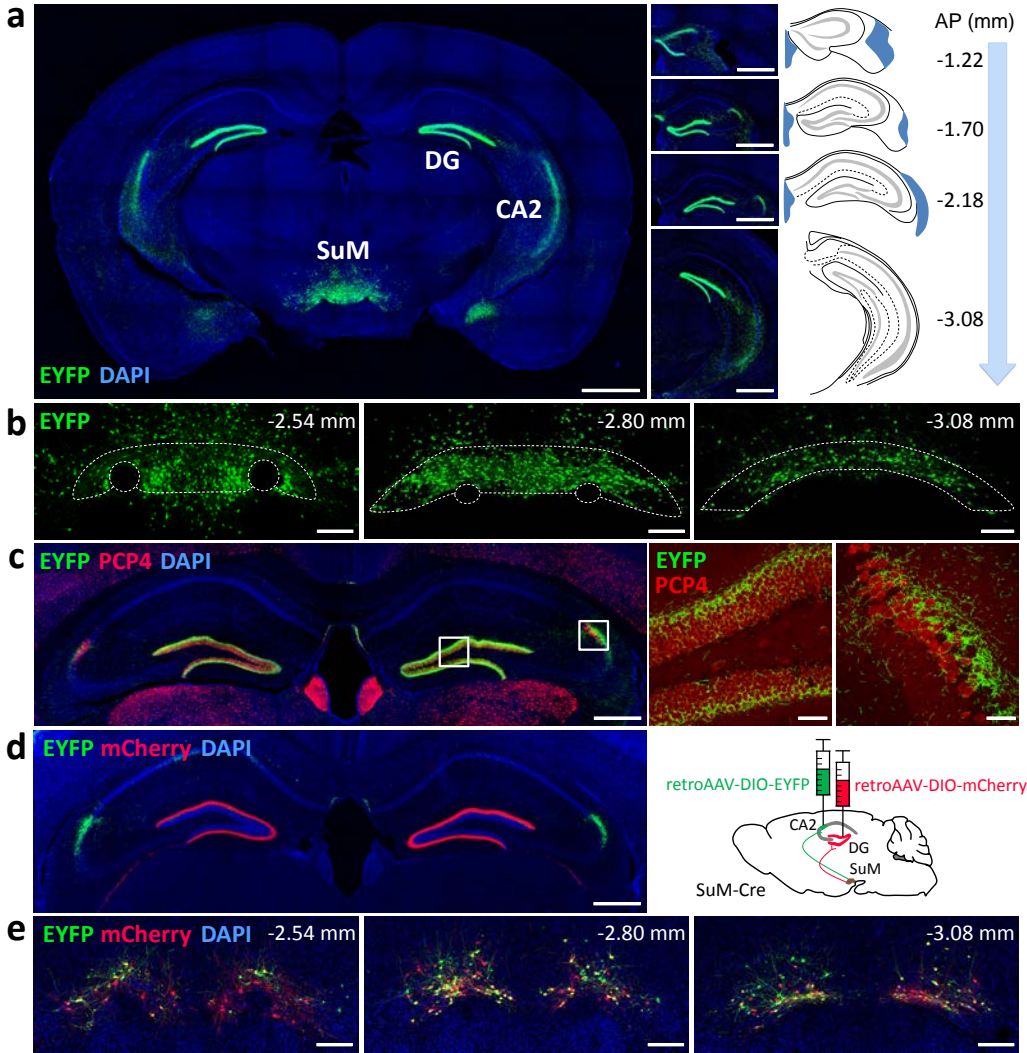
a
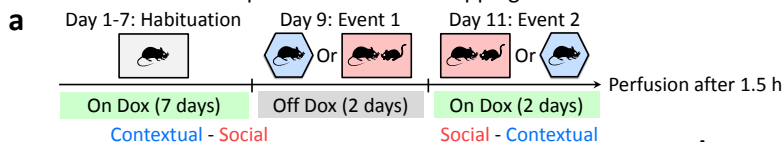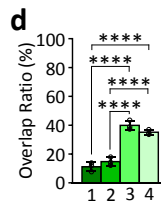Familiar → Contextual

Familiar → Social

b
SuM

Familiar

Contextual

Social

c
c-Fos+ cells per mm²

Familiar
Contextual
Social

****
****

d
Familiar → Contextual → Familiar → Social

e
SuM

f

Cell No.	Familiar	FR (Hz)	Contextual	FR (Hz)	Social	FR (Hz)
1		2.5		3.8		1.0
2		0.2		0.6		0.2
3		1.4		0.8		7.5
4		0.6		0.6		1.3
5		3.3		8.2		6.2
6		0.2		0.8		0.8

10 s

g
Mean FR of all pEN (Hz)

****
*

h
Mean FR in Familiar (Hz)
Mean FR in Contextual (Hz)
21.8%
8.4%

i
Mean FR in Familiar (Hz)
Mean FR in Social (Hz)
21.0%
0.8%

j
Contextual Increase 14
12
Social Increase 13

k
FR (% of Familiar mean)
Time (min)

Contextual
Social
Familiar

Significant increase | Significant decrease | No significant change

a

EYFP DAPI

DG
CA2
SuM

AP (mm)
-1.22
-1.70
-2.18
-3.08

b

EYFP

-2.54 mm   -2.80 mm   -3.08 mm

c

EYFP PCP4 DAPI

EYFP
PCP4

d

EYFP mCherry DAPI

retroAAV-DIO-EYFP   retroAAV-DIO-mCherry

CA2
DG
SuM
SuM-Cre

e

EYFP mCherry DAPI   -2.54 mm   -2.80 mm   -3.08 mm

Event-specific c-Fos+ cells mapping

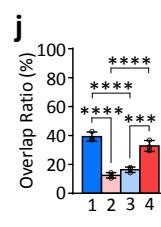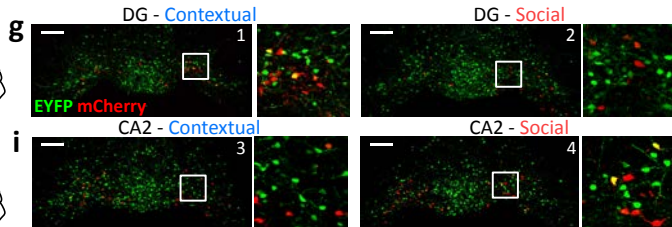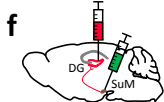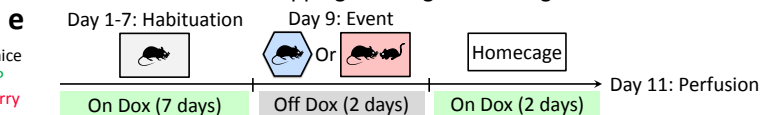**a** Day 1-7: Habituation | Day 9: Event 1 | Day 11: Event 2 → Perfusion after 1.5 h

On Dox (7 days) | Off Dox (2 days) | On Dox (2 days)

b SuM-Cre/c-fos-tTA mice
AAV-TRE-DIO-EYFP

c Contextual - Social | Social - Contextual
Contextual - Contextual | Social - Social
EYFP c-Fos

d Overlap Ratio (%)
****

c-Fos+ cells mapping & retrograde tracing

e Day 1-7: Habituation | Day 9: Event | Homecage → Day 11: Perfusion

On Dox (7 days) | Off Dox (2 days) | On Dox (2 days)

SuM-Cre/c-fos-tTA mice
AAV-TRE-DIO-EYFP
retroAAV-DIO-mCherry

f DG SuM

g DG - Contextual | DG - Social
EYFP mCherry

h CA2 SuM

i CA2 - Contextual | CA2 - Social

j Overlap Ratio (%)
****

Circuit-specific optogenetic identification and recording

k OptoID → Familiar → Contextual → Familiar → Social

SuM-Cre mice
AAV-DIO-ChR2-EYFP

l DG SuM

m Spikes per sec

n 50 µV / 200 µs

o CA2 SuM

p Spikes per sec
Time (ms)

q

r Cell No. | FR (Hz)
1 4.9
2 1.5
3 0.9
4 5.0
1 7.3
2 6.8
3 0.6
4 4.8
1 4.6
2 4.9
3 1.4
4 7.3
10 s

s FR Change
○ Contextual ○ Social
**

t FR Change
***

a

15 min → 15 min → 15 min → laser 15 min → laser 15 min →

A1   A2   A3   A4   B1   B2

b SuM-DG activation
AAV-DIO-ChR2-EYFP

Distance Traveled (%)

A1 A2 A3 A4 B1 B2

*

c SuM-DG inhibition
AAV-DIO-eNpHR-EYFP

Distance Traveled (%)

A1 A2 A3 A4 B1 B2

****

d SuM-CA2 activation
AAV-DIO-ChR2-EYFP

Distance Traveled (%)

A1 A2 A3 A4 B1 B2

e SuM-CA2 inhibition
AAV-DIO-eNpHR-EYFP

Distance Traveled (%)

A1 A2 A3 A4 B1 B2

— EYFP, control — ChR2, activation — eNpHR, inhibition

f

Stimulus → 1 h → laser Familiar

i

Stimulus → 1 h → laser Novel

g SuM-DG

Habitation Index   n.s.   Habitation Index   n.s.

j SuM-DG

Habitation Index   n.s.   Habitation Index   n.s.

h SuM-CA2

Habitation Index   ***   Habitation Index   n.s.

k SuM-CA2

Habitation Index   n.s.   Habitation Index   n.s.

☐ EYFP, control ☐ ChR2, activation ☐ eNpHR, inhibition

a

c-Fos+ cells per mm^2

Legend: Control (white), Contextual (blue), Social (red)

Regions: SuM, DMH, LHA, MPN, PH, MM, PVH, MPO, VMH, LPO, AHN

Significance markers: SuM ****; DMH ****; LHA ****; MPN ****; PH ****; MM ****; PVH ****; MPO **** and *; VMH ****; LPO **** and n.s.; AHN *** and **

b

AP -0.3 mm	Control	Contextual	Social
AP -0.8 mm			
AP -1.3 mm			
AP -1.8 mm			
AP -2.3 mm			
AP -2.8 mm			

Labels within sections: PVH, LPO, MPN, MPO (AP -0.3 mm); LHA, AHN (AP -0.8 mm); LHA, DMH, VMH (AP -1.3 mm); LHA, PH, DMH (AP -1.8 mm); LHA, PH (AP -2.3 mm); PH, SuM, MM (AP -2.8 mm)

a

SuM

b

c

SNr VTA PH VTA SNr
cp
LH **SuM** LH cp
LM MM LM
AP -2.54 mm

VTA PH VTA
SNc
SNr SNr
cp
LM **SuM** LM
LM MM LM
AP -2.80 mm

VTA PH VTA
SNr SNc SNc SNr
cp **SuM** cp
LM MM LM
AP -3.08 mm

● In target area   ● Out of target area

d

Familiar → Contextual → Familiar → Social

e

Mean FR of all pIN (Hz)

n.s.
n.s.

f

Mean FR in Familiar (Hz)

13.6%   4.5%

Mean FR in Contextual (Hz)

g

Mean FR in Familiar (Hz)

13.6%   4.5%

Mean FR in Social (Hz)

h

Contextual Increase
2

1

Social Increase
2

■ Significant increase   ■ Significant decrease   ■ No significant change

a

Directly 5' of csf2rb2 start codon | Directly 3' of csf2rb2 start codon

50 bp 5' primer — Cre — FRT — Amp^R — FRT — 50 bp 3' primer

csf2rb2 promoter

BAC clone RP23.233L7 (197245 bp)

RedET recombination

csf2rb2 promoter — Cre — FRT — Amp^R — FRT'

BAC clone RP23.233L7 (197245 bp)

FLP recombination (for deletion of Amp^R)

csf2rb2 promoter — Cre

BAC clone RP23.233L7 (197245 bp)

b

Cre — AP -2.80 mm

c

AP -1.60 mm — Hilus / CA3 / BLA — Hilus / CA3

AP -1.94 mm — Hilus / CA3 / BLA — BLA

AP -2.30 mm — Hilus / PF / PH / LHA / CA3 — PF / PH / LHA

AP -2.54 mm — Hilus / PAG / RL / SuM / CA3 — PAG

AP -2.80 mm — Hilus / PAG / SuM / CA3 — SuM

AP -3.08 mm — Hilus / PAG / RL / SuM — RL / SuM

AP -3.40 mm — PAG / RL / Hilus — Hilus

d

Lateral: 0.05 mm — RL / SuM

Lateral: 0.23 mm — PF / SuM

Lateral: 0.68 mm — Hilus / SuM

Lateral: 1.10 mm — Hilus

Lateral: 1.73 mm — Hilus / CA3

Lateral: 2.15 mm — Hilus / CA3

Lateral: 2.52 mm — Hilus / CA3 / CA3

a

AP +1.10 mm — IG, DP, LS, AcbSh, MS

AP +0.86 mm — IG, SHi, LS, AcbSh, MS

AP +0.14 mm — IG, SFi, LS, MPO, LPO

AP −0.82 mm — IG, VRe, MD, RE, AHN, LHA

AP −1.06 mm — CA2, DG, CM, MDl, IAM, RE, AHN, LHA, fi

AP −1.70 mm — CA2, DG, RE, LHA, fi

AP −1.82 mm — CA2, DG, RE, LHb, LHA

AP −2.06 mm — CA2, DG, LHb, LHA, PH, fi

AP −2.30 mm — DG, CA2, PH, LHA

AP −2.54 mm — DG, CA2, SuM

AP −2.80 mm — DG, SuM

AP −3.08 mm — DG, SuM

2 mm

b

Lateral: 0.23 mm — CA2, DG, SuM

Lateral: 0.68 mm — CA2, DG, SuM

Lateral: 1.10 mm — CA2, DG

Lateral: 1.63 mm — CA2, DG

Lateral: 2.15 mm — CA2, DG

Lateral: 2.73 mm — CA2, DG

Lateral: 3.33 mm — CA2, DG

c

Horizontal (Top → Bottom) — CA2, Septum, DG, SuM

Horizontal (Bottom → Top) — Acb, CA2, DG, SuM

Sagittal (Lateral → Medial) — CA2, DG, EC, Acb, SuM

d

#1263 (Contextual) — YFP, Reflection
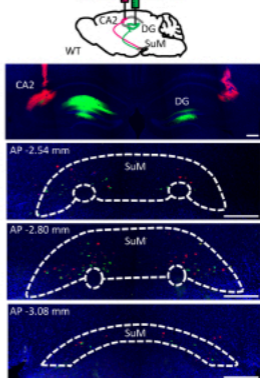
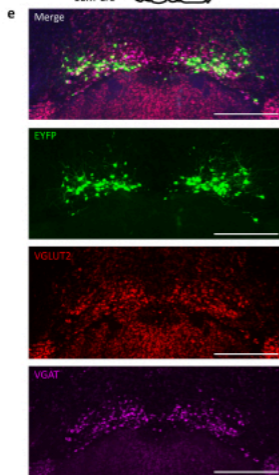#1265 (Social) — YFP, Reflection

YFP
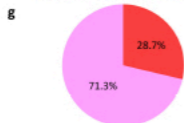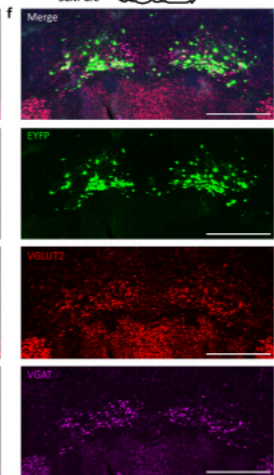
c-Fos

Merge

a retroAAV-DIO-EYFP   retroAAV-DIO-mCherry

b CTB 594   CTB 488

c retroAAV-DIO-EYFP

d retroAAV-DIO-EYFP

e Merge / EYFP / VGLUT2 / VGAT
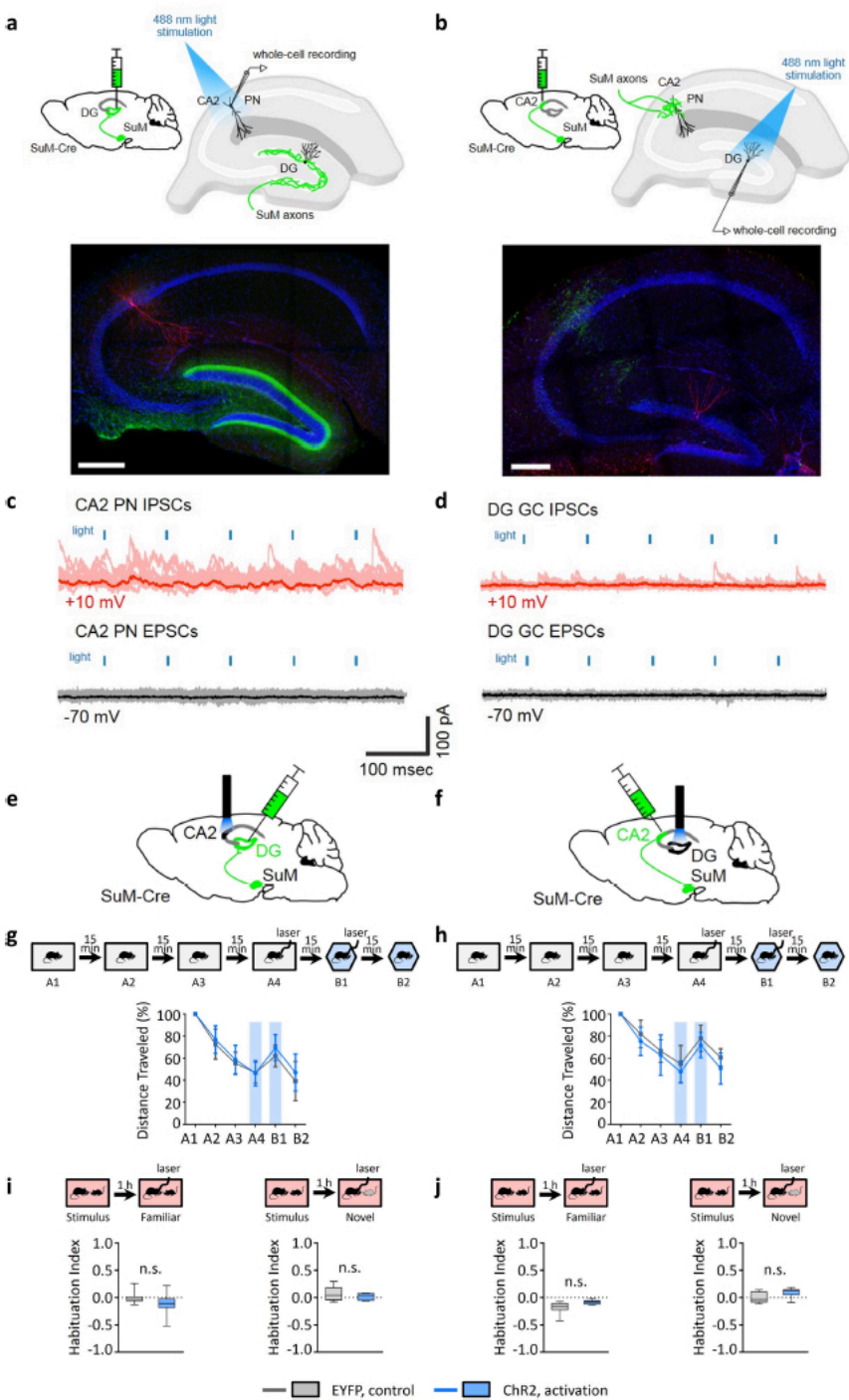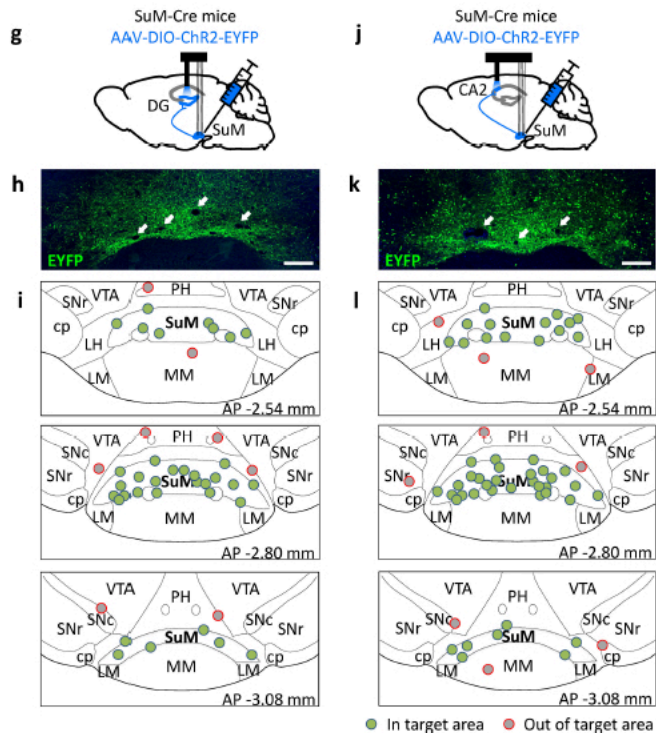
f Merge / EYFP / VGLUT2 / VGAT

g

h

EYFP+/VGLUT2+/VGAT-
EYFP+/VGLUT2+/VGAT+

28.7%
71.3%

13.1%
86.9%

a 488 nm light stimulation — whole-cell recording — CA2 PN — SuM-Cre — DG — SuM — SuM axons

b 488 nm light stimulation — CA2 — SuM axons — PN — SuM-Cre — SuM — DG — whole-cell recording

c
CA2 PN IPSCs
light
+10 mV

CA2 PN EPSCs
light
−70 mV

d
DG GC IPSCs
light
+10 mV

DG GC EPSCs
light
−70 mV

100 pA
100 msec

e CA2 — DG — SuM — SuM-Cre

f CA2 — DG — SuM — SuM-Cre

g
A1 →15 min→ A2 →15 min→ A3 →15 min→ A4 (laser) →15 min→ B1 (laser) →15 min→ B2

Distance Traveled (%)
A1 A2 A3 A4 B1 B2

h
A1 →15 min→ A2 →15 min→ A3 →15 min→ A4 (laser) →15 min→ B1 (laser) →15 min→ B2

Distance Traveled (%)
A1 A2 A3 A4 B1 B2

i
Stimulus →1 h→ Familiar (laser)
Habituation Index — n.s.

Stimulus →1 h→ Novel (laser)
Habituation Index — n.s.

j
Stimulus →1 h→ Familiar (laser)
Habituation Index — n.s.

Stimulus →1 h→ Novel (laser)
Habituation Index — n.s.

— EYFP, control   — ChR2, activation

c-Fos+ cells mapping & retrograde tracing

a

Day 1-7: Habituation

Day 8: Event

Or

Perfusion after 1.5 h

SuM-Cre mice
retroAAV-DIO-EYFP

b

DG

SuM

c

DG - Contextual

1

DG - Social

2

EYFP c-Fos

d

CA2

SuM

e

CA2 - Contextual

3

CA2 - Social

4

f

Overlap Ratio (%)

g

SuM-Cre mice
AAV-DIO-ChR2-EYFP

DG

SuM

j

SuM-Cre mice
AAV-DIO-ChR2-EYFP

CA2

SuM

h

EYFP

k

EYFP

i

SNr VTA PH VTA SNr
cp   cp
LH   SuM   LH
LM   MM   LM
AP -2.54 mm

SNc VTA PH VTA SNc
SNr   SNr
cp   SuM   cp
LM   MM   LM
AP -2.80 mm

VTA PH VTA
SNr SNc   SNc SNr
cp   SuM   cp
LM   MM   LM
AP -3.08 mm

l

SNr VTA PH VTA SNr
cp   cp
LH   SuM   LH
LM   MM   LM
AP -2.54 mm

SNc VTA PH VTA SNc
SNr   SNr
cp   SuM   cp
LM   MM   LM
AP -2.80 mm

VTA PH VTA
SNr SNc   SNc SNr
cp   SuM   cp
LM   MM   LM
AP -3.08 mm

In target area   Out of target area

a Context A   Context B

b A1 → 15 min → A2 → 15 min → A3 → 15 min → A4 (laser) → 15 min → B1 (laser) → 15 min → B2

c DG-ChR2

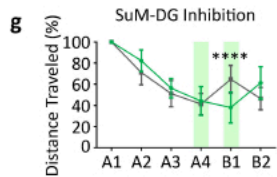|					
Distance (m)	15.722	12.853	7.124	6.988	9.465	6.944
Relative Ratio (%)	100%	81.75%	45.31%	44.44%	60.20%	44.17%

d DG-eNpHR

Distance (m)	17.138	13.064	9.038	7.965	7.167	8.651
Relative Ratio (%)	100%	76.23%	52.74%	46.48%	41.82%	50.48%

e DG-EYFP

Distance (m)	11.985	9.124	6.596	5.572	9.334	5.542
Relative Ratio (%)	100%	76.13%	55.04%	46.49%	77.88%	46.24%

f SuM-DG Activation

g SuM-DG Inhibition

h SuM-CA2 Activation

i SuM-CA2 Inhibition
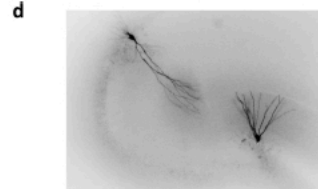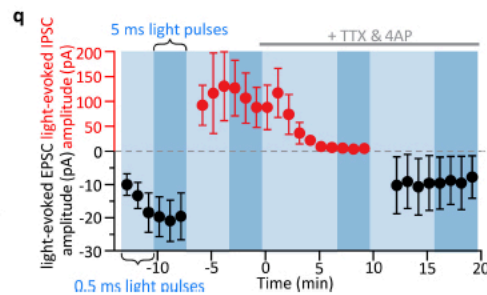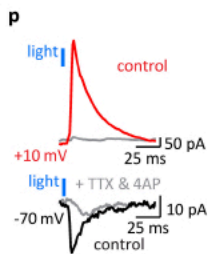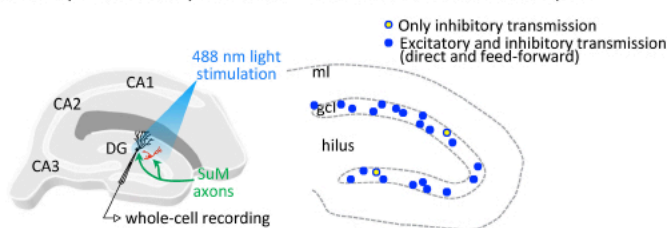
No laser, control   ChR2, activation   eNpHR, inhibition
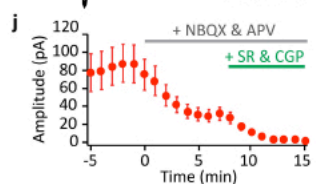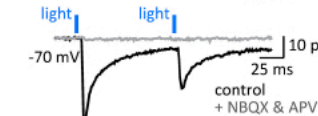
a Direct glutamatergic transmission in area CA2 from SuM inputs

488 nm light stimulation

SuM axons

whole-cell recording

CA2 PN CA1

CA3 DG

so, sp, sr

CA2, CA1, CA3a, CA3b, mf

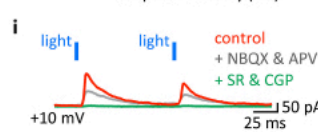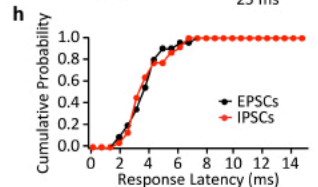- Direct glutamatergic transmission
- unconnected
- CA1 PN
- CA2 PN
- CA3 PN

b Feed-forward inhibitory transmission in area CA2 from SuM inputs

488 nm light stimulation

SuM axons

whole-cell recording

IN

CA2, CA1, CA3

- Feed-forward inhibitory transmission
- unconnected
- CA1 PN
- CA2 PN
- CA3 PN

c Excitatory and inhibitory transmission onto DG GC cells from SuM inputs

488 nm light stimulation

SuM axons

whole-cell recording

ml, gcl, hilus

- Only inhibitory transmission
- Excitatory and inhibitory transmission (direct and feed-forward)

f SuM-DG Transmission

whole-cell recording

488 nm light stimulation

SuM axons

GC, IN

g light, +10 mV, -70 mV, 50 pA, 25 ms

h Cumulative Probability vs Response Latency (ms), EPSCs, IPSCs

i light, light, control, + NBQX & APV, + SR & CGP, +10 mV, 50 pA, 25 ms; light, light, -70 mV, 10 pA, 25 ms, control, + NBQX & APV

j Amplitude (pA) vs Time (min), + NBQX & APV, + SR & CGP

k SuM-CA2 Transmission

488 nm light stimulation

SuM axons

whole-cell recording

IN, PN

l light, +10 mV, -70 mV, 50 pA, 25 ms

m Cumulative Probability vs Response Latency (ms), EPSCs, IPSCs

n light, light, control, + NBQX & APV, +10 mV, 50 pA, 25 ms; light, light, -70 mV, 10 pA, 25 ms, control, + NBQX & APV

o Amplitude (pA) vs Time (min), + NBQX & APV

p light, control, +10 mV, 50 pA, 25 ms; light, -70 mV, 10 pA, 25 ms, + TTX & 4AP, control

q light-evoked EPSC amplitude (pA) / light-evoked IPSC amplitude (pA) vs Time (min), 5 ms light pulses, + TTX & 4AP, 0.5 ms light pulses

a
retroAAV-DIO-TVA
retroAAV-DIO-GFP-oG
EnvA+RV*dG*-mCherry
DG
SuM

b
retroAAV-DIO-TVA
retroAAV-DIO-GFP-oG
EnvA+RV*dG*-mCherry
CA2
SuM

c SuM

d SuM

e
PVH
ZI
PH
LH
MS
PH
LH
LS
MS
PAG
MRN
VTA
SI
MPO
LPO
PAG
AcbSh
MRN
DR
MnR

f
PVH
ZI
PH
LH
MS
PH
LH
LS
MS
PAG
MRN
VTA
SI
MPO
LPO
PAG
AcbSh
MRN
DR
MnR

g DG-projecting SuM neurons

LS
MS
SI
AcbSh
ZI
LHA
MPO
LPO
PVH
PH
PAG
MRN
VTA
Raphe

Fraction of total input
0.4 0.3 0.2 0.1 0.0

h CA2-projecting SuM neurons

LS
MS
SI
AcbSh
ZI
LHA
MPO
LPO
PVH
PH
PAG
MRN
VTA
Raphe

Fraction of total input
0.0 0.1 0.2 0.3 0.4